



Modeling multicomponent ionic transport in groundwater with IPhreeqc coupling: Electrostatic interactions and geochemical reactions in homogeneous and heterogeneous domains

Muniruzzaman, Muhammad; Rolle, Massimo

Published in:
Advances in Water Resources

Link to article, DOI:
[10.1016/j.advwatres.2016.10.013](https://doi.org/10.1016/j.advwatres.2016.10.013)

Publication date:
2016

Document Version
Peer reviewed version

[Link back to DTU Orbit](#)

Citation (APA):
Muniruzzaman, M., & Rolle, M. (2016). Modeling multicomponent ionic transport in groundwater with IPhreeqc coupling: Electrostatic interactions and geochemical reactions in homogeneous and heterogeneous domains. *Advances in Water Resources*, 98, 1-15. <https://doi.org/10.1016/j.advwatres.2016.10.013>

General rights

Copyright and moral rights for the publications made accessible in the public portal are retained by the authors and/or other copyright owners and it is a condition of accessing publications that users recognise and abide by the legal requirements associated with these rights.

- Users may download and print one copy of any publication from the public portal for the purpose of private study or research.
- You may not further distribute the material or use it for any profit-making activity or commercial gain
- You may freely distribute the URL identifying the publication in the public portal

If you believe that this document breaches copyright please contact us providing details, and we will remove access to the work immediately and investigate your claim.

This is a Post Print of the article published on line 13th October 2016 in Advances in Water Resources and printed December 2016, 98, 1-15. The publishers' version is available at the permanent link: <http://dx.doi.org/10.1016/j.advwatres.2016.10.013>

Modeling multicomponent ionic transport in groundwater with IPhreeqc coupling: electrostatic interactions and geochemical reactions in homogeneous and heterogeneous domains

Muhammad Muniruzzaman¹ and Massimo Rolle^{1,2*}

¹Center for Applied Geosciences, University of Tübingen, Hölderlinstr. 12, D-72074
Tübingen, Germany

²Department of Environmental Engineering, Technical University of Denmark,
Miljøvej, Building 115, 2800 Kgs. Lyngby, Denmark

*Corresponding author phone: +45 45251566; email: masro@env.dtu.dk

Highlights

- 2-D code for multicomponent ionic transport including Coulombic interactions.
- Geochemical reactions implemented with IPhreeqc coupling.
- Applications in physically and chemically heterogeneous domains.

1 **ABSTRACT**

2 The key role of small-scale processes like molecular diffusion and electrochemical
3 migration has been increasingly recognized in multicomponent reactive transport in
4 saturated porous media. In this study, we propose a two-dimensional multicomponent
5 reactive transport model taking into account the electrostatic interactions during transport
6 of charged ions in physically and chemically heterogeneous porous media. The modeling
7 approach is based on the local charge balance and on the description of compound-
8 specific and spatially variable diffusive/dispersive fluxes. The multicomponent ionic
9 transport code is coupled with the geochemical code PHREEQC-3 by utilizing the
10 IPhreeqc module, thus enabling to perform the geochemical calculations included in the
11 PHREEQC's reaction package. The multicomponent reactive transport code is
12 benchmarked with different 1-D and 2-D transport problems. Successively, conservative
13 and reactive transport examples are presented to demonstrate the capability of the
14 proposed model to simulate transport of charged species in heterogeneous porous media
15 with spatially variable physical and chemical properties. The results reveal that the
16 Coulombic cross-coupling between dispersive fluxes can significantly influence
17 conservative as well as reactive transport of charged species both at the laboratory and at
18 the field scale.

19 **Keywords:** *multicomponent diffusion, electrochemical migration, IPhreeqc coupling,*
20 *Coulombic interactions, reactive transport modeling*

21

1. INTRODUCTION

The importance of coupling subsurface solute transport models with geochemical codes, capable of simulating a wide variety of equilibrium and kinetic reactions, has been increasingly recognized and has led to major developments of reactive transport codes for subsurface environmental simulation (e.g., [1,2]). The coupling of fluid flow, mass transport and geochemical reactions is instrumental for understanding and predicting the complex interplay between physical and bio-geochemical processes in sediments and groundwater systems, as well as for the quantitative interpretation of experimental observations both at the laboratory and field scales. Combining flow and transport codes with geochemical reaction packages has led to a first generation of now well-established reactive transport simulators for both groundwater (e.g., CrunchFlow [3]; Geochemist's Workbench [4]; PHT3D [5]; PHAST [6]) and unsaturated/multiphase flow (e.g., HYDROGEOCHEM [7]; TOUGHREACT [8-10]; MIN3P [11]). Developments have continued over the last decade with increasing capabilities added to existing simulators as well as new couplings between different transport and geochemical codes (e.g. HP1/HPx [12]; PHWAT [13]; RICH-PHREEQC [14]). Impetus to such advances was certainly provided by the release of modules such as IPhreeqc [15] and PhreeqcRM [16] devised to increase the flexibility in interfacing the widely used USGS's geochemical reaction package PHREEQC [17,18] with other codes. In particular, IPhreeqc is a C++ PHREEQC module designed for coupling PHREEQC's reaction capabilities (e.g., equilibrium reactions, ion exchange, surface complexation, solid solutions, mineral dissolution and precipitation, as well as kinetic reactions both abiotic and microbially mediated) to other software programs (for example, MATLAB[®], Excel[®], Visual Basic[®])

45 and/or programming and scripting languages (for instance, C, C++, FORTRAN, Python,
46 R). IPhreeqc offers a wide range of extensive features to combine multidimensional
47 transport simulators with comprehensive geochemistry packages including
48 thermodynamic databases [19,20]. Recent reactive transport simulators that benefited
49 from the IPhreeqc capabilities include the couplings with COMSOL Multiphysics® (e.g.,
50 [19]; [21,22]), OpenGeoSys [23,24] and UTCHEM [25].

51 In this study we also take advantage of the IPhreeqc capabilities to explore the coupling
52 between a two-dimensional multicomponent ionic formulation of charged species
53 advective-dispersive transport and reactive processes. Many studies have demonstrated
54 the importance of electrostatic effects due to charge interactions and leading to
55 multicomponent diffusion of ions in aqueous solutions. Experimental observations have
56 shown the effects of Coulombic interactions on the diffusive mobility of major ions,
57 heavy metals and radioactive tracers both at the laboratory [26,27] and at the field scale
58 [28-31]. The description of such interactions in multicomponent diffusion models is
59 usually treated by including an electromigration term in addition to the classical Fickian
60 diffusion term (e.g., [32-36]). In a series of recent laboratory flow-through experiments
61 we have shown that the role of Coulombic effects is critical not only in diffusion-
62 dominated systems but also in advection-dominated flow regimes [37-39]. In fact, the
63 results of such experiments demonstrated that the displacement of ions in porous media is
64 coupled and the electromigration effects do not vanish at high flow velocities. These
65 experimental findings represent a challenge as well as an opportunity for further
66 development of reactive transport codes. Only recently a dataset of multicomponent
67 conservative ionic transport obtained under flow-through conditions in a homogeneous

porous medium has been used to benchmark the multicomponent transport capabilities of the CrunchFlow and MIN3P codes [40]. However, to the best of our knowledge, the behavior and effects of Coulombic interactions for multidimensional conservative and reactive transport in physically and chemically heterogeneous porous media have not been investigated, yet. The purpose of this contribution is to present a reactive transport tool helping to address these issues in particular on the light of the increased recognition of the key role of molecular diffusion for solute transport from the pore to the field scale. Small scale diffusive processes have been shown to impact solute transport in flow-through systems not only at the laboratory (e.g., [41-45]) but also at the larger field scale (e.g., [46-54]). The impact of diffusion, which is the only true mixing process in groundwater [55], on solute transport indeed does not vanish at larger scales but propagates through scales also under flow-through conditions [53]. Models aiming at capturing these effects in heterogeneous flow fields need to implement improved and more realistic descriptions of local dispersion, linking the mechanical dispersion term to spatially-variable hydraulic conductivity values and avoiding using constant dispersivities that inevitably mask (or underestimate) the role of aqueous diffusion in porous media.

This work presents a two-dimensional reactive transport model that explicitly accounts for the Coulombic interactions coupled with geochemical reactions during multicomponent ionic transport in both homogeneous and heterogeneous flow-fields under transient transport conditions. The modeling approach is based on a charge-balanced multicomponent formulation and on the spatially variable description of local hydrodynamic dispersion that is of key importance for the coupling of the fluxes of the different ionic species in solution. Additionally, we couple the two-dimensional

multicomponent ionic transport model with the widely used geochemical code PHREEQC (version 3, [18]) by using the reaction module IPhreeqc [15]. Thus, the proposed numerical reactive-transport model provides a comprehensive framework that is based on the novel combination of three specific features: (i) detailed description of spatially variable local hydrodynamic dispersion, (ii) multicomponent ionic formulation; and (iii) extensive reaction capabilities through the coupling with PHREEQC. These features represent distinctive and unique characteristics for a reactive transport simulator and are particularly advantageous for performing transport simulations in physically and chemically heterogeneous domains. The 2-D multicomponent model is systematically benchmarked with the analytical solution of a 2-D transport problem, with experimental data, and with 1-D reactive transport scenarios solved in PHREEQC. Successively, application examples, with different levels of complexity, are presented to illustrate transient multicomponent ionic transport and the influence of charge interactions in both conservative and reactive systems in homogeneous and heterogeneous porous media.

2. MULTICOMPONENT IONIC TRANSPORT

The most distinguishing feature of aqueous diffusion of charged species compared to non-charged solutes is the electrostatic interactions between the dissolved charged species and/or with charged interfaces. Multicomponent ionic diffusion models are generally used to account for these inter-species interactions during diffusive movement of charged species at different scales (e.g., [27-29]; [32,33]; [35]; [56-59]). These models, based on Nernst-Planck formulations, are typically derived from the chemical potential

expressions by following a pragmatic extension of Fick's law (e.g., [35,36,60]).
 Therefore, the multicomponent diffusive movement of a charged species in electrolyte
 systems can be expressed as [29,36]:

$$J_i = -D_i \nabla C_i - D_i C_i \nabla \ln \gamma_i - D_i \frac{z_i F}{RT} C_i \nabla \Phi \quad i = 1, 2, 3, \dots, N \quad (1)$$

where D_i is the self-diffusion coefficient, C_i is the concentration of charged species i , γ_i is
 the activity coefficient, z_i is the charge number, F is the Faraday's constant, R is the ideal
 gas constant, T is the temperature, Φ is the electrostatic potential, and N is the number of
 species.

In dilute solutions and in the absence of strong ionic strength gradients, the gradient of
 the activity coefficients (second term of Eq. 1) can be neglected [33]. Thus, the above
 expression describing the multicomponent ionic diffusive fluxes reduces to:

$$J_i = -D_i \nabla C_i - D_i \frac{z_i F}{RT} C_i \nabla \Phi \quad (2)$$

This equation includes fluxes due to self-diffusion as well as electromigration, which is
 basically induced from the electrostatic interactions, for a particular mobile species.

Following two physical constraints based on electroneutrality (i.e., (i) conservation of

local charge balance, $\sum_{i=1}^N z_i C_i = 0$ and/or (ii) zero influx of electrical current, $\sum_{i=1}^N z_i J_i = 0$

), the gradient of Φ can be expressed as:

$$\nabla\Phi = \frac{\sum_{i=1}^N (z_i D_i \nabla C_i)}{\sum_{i=1}^N (z_i^2 F D_i C_i) / RT} \quad (3)$$

Therefore, the flux expression of Eq. (2) readily reduces to:

$$J_i = -D_i \nabla C_i + \frac{z_i D_i C_i}{\sum_{j=1}^N (z_j^2 D_j C_j)} \sum_{k=1}^N (z_k D_k \nabla C_k) \quad (4)$$

This formulation directly describes the movement of a particular charged species as a function of concentration gradients, self-diffusion coefficients, and charge numbers not only of that ion but also of all ionic species in the electrolyte system. Eq. (4) can also be further rearranged in a more compact notation that takes the form:

$$J_i = -\sum_{j=1}^N (D_{ij} \nabla C_j) \quad (5)$$

where D_{ij} are the inter-diffusion coefficients that include both the pure diffusive (first term, Eq. 4) and the electromigration (second term, Eq. 4) fluxes. The cross-coupled inter-diffusion coefficients are defined as:

$$D_{ij} = \delta_{ij} D_i - \frac{z_i z_j D_i D_j C_i}{\sum_{k=1}^n (z_k^2 D_k C_k)} \quad (6)$$

where δ_{ij} is the Kronecker delta that is equal to 1 when $i=j$ and equal to 0 if $i \neq j$.

In flow-through systems an analogous set of equations (Eqs. 1-6) can be derived by following the above steps and replacing the pure self-diffusion coefficients by the hydrodynamic dispersion coefficients [37,38].

3. MODELING APPROACH

The proposed model is implemented in MATLAB[®] and allows for steady-state flow, transient multicomponent advective-dispersive transport and geochemical reactions, the latter performed with the IPhreeqc coupling. Fig. 1 schematically illustrates the structure of the multicomponent reactive transport code. Details on the model capabilities, in particular the multicomponent ionic transport features and the coupling with the geochemical reaction package, are discussed in the sections below.

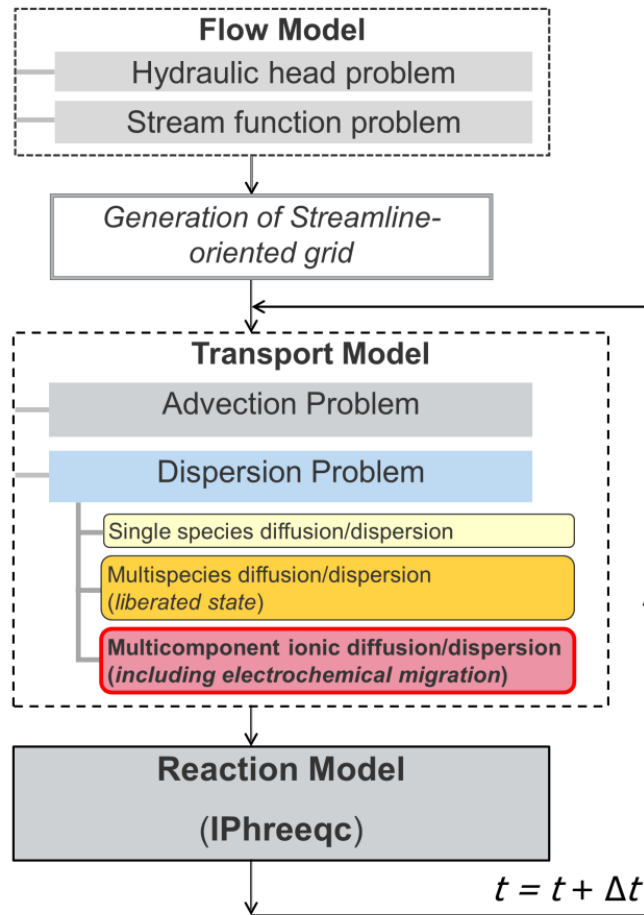


Figure 1: Schematic diagram of the structure of the multicomponent reactive transport model.

151 3.1 Solution of Flow and Transport Equations

152 The governing equation for steady-state groundwater flow in a two-dimensional domain
 153 is expressed as [61]:

$$\begin{aligned}\nabla \cdot (\mathbf{K} \nabla h) &= 0 \\ \nabla \cdot (\mathbf{K}^{-1} \nabla \psi) &= 0\end{aligned}\tag{7}$$

154 where h , ψ and \mathbf{K} are hydraulic head, stream function and hydraulic conductivity tensor,
 155 respectively. The groundwater flow problem (Eq. 7) is solved numerically by bilinear
 156 finite elements on rectangular grid.

157 The governing equation for multicomponent ionic transport problem coupled with
 158 reactive processes in two-dimensional saturated porous media reads as:

$$\frac{\partial C_i}{\partial t} = -\mathbf{v} \cdot \nabla C_i + \nabla \cdot \left(\sum_{j=1}^N \mathbf{D}_{ij} \nabla C_j \right) - R_i\tag{8}$$

159 where t is time, \mathbf{v} is the seepage velocity vector, \mathbf{D}_{ij} is the tensor for cross-coupled
 160 dispersion coefficients, R_i is the reactive source/sink term. For charged compounds the
 161 entries of \mathbf{D}_{ij} in a two-dimensional local coordinate system, referencing along the
 162 directions parallel and orthogonal to flow, are described as:

$$\mathbf{D}_{ij} = \begin{bmatrix} \mathbf{D}_{ij}^L & 0 \\ 0 & \mathbf{D}_{ij}^T \end{bmatrix}\tag{9}$$

163 in which \mathbf{D}_{ij}^L and \mathbf{D}_{ij}^T are the matrices of longitudinal and transverse cross-coupled
 164 dispersion coefficients [38], respectively. These cross-coupled terms, which allow
 165 accounting for the flux of a charged species driven by both its own concentration gradient

166 and the electrical field created by the movement of other ions present in solution, are in
 167 fact analogous to inter-diffusion coefficients in Eq. (6) and can be expressed as:

$$\begin{aligned} \mathbf{D}_{ij}^L &= \delta_{ij} D_i^L - \frac{z_i z_j D_i^L D_j^L C_i}{\sum_{k=1}^N (z_k^2 D_k^L C_k)} \\ \mathbf{D}_{ij}^T &= \delta_{ij} D_i^T - \frac{z_i z_j D_i^T D_j^T C_i}{\sum_{k=1}^N (z_k^2 D_k^T C_k)} \end{aligned} \quad (10)$$

168 where D_i^L and D_i^T are the longitudinal and transverse hydrodynamic self-dispersion
 169 coefficient of species i (i.e., when a particular ion is “liberated” from the other charged
 170 species in solution). The hydrodynamic dispersion coefficients, which are important
 171 parameters for the realistic description of dispersive transport, are parameterized by using
 172 the linear relationship proposed by Guedes de Carvalho and Delgado [62] for longitudinal
 173 dispersion and a non-linear compound-specific relationship [50,63] for the transverse
 174 component:

$$\begin{aligned} D_i^L &= D_i^P + \frac{1}{2} v d \\ D_i^T &= D_i^P + D_i^{aq} \left(\frac{Pe_i^2}{Pe_i + 2 + 4\delta^2} \right)^\beta \end{aligned} \quad (11)$$

175 where D_i^{aq} is the aqueous diffusion coefficient, $D_i^P = D_i^{aq} / \tau$ is the pore diffusion
 176 coefficient and τ the tortuosity of the porous medium. Since the latter is difficult to
 177 determine, the pore diffusion coefficient is typically described as a function of the
 178 porosity (θ) and a common approximation for unconsolidated material is $D_i^P \approx \theta D_i^{aq}$
 179 (e.g., Archie [64]; Boving and Grathwohl[65]). d is the average grain size diameter and

180 $Pe_i (= vd / D_i^{aq}$; with v being the flow velocity) is the grain Péclet number of species i . δ
 181 denotes the ratio between the length of a pore channel to its hydraulic radius. β is an
 182 empirical exponent that accounts for the effects of incomplete mixing in the pore
 183 channels. The parameterizations of D_i^L and D_i^T in Eq. 11 were selected because they
 184 have been validated and extensively supported by experimental data from controlled
 185 flow-through experiments. Other parameterizations such as the classic model of
 186 Scheidegger [66] as well as more complex models of local dispersion obtained for
 187 instance from pore-scale analysis and suggesting a weak non-linearity also of the
 188 longitudinal component [67] can be readily implemented. An important feature for high-
 189 resolution transport simulations in heterogeneous porous media is to take into account
 190 that the grain diameter (d) in Eq. (11) is spatially variable and should be linked to the
 191 local hydraulic conductivity value. We use the simple approximation of Hazen [68],
 192 which was adopted in previous studies (e.g., [51,69]), as a relationship between the grain
 193 diameter and hydraulic conductivity:

$$d \approx c\sqrt{K} \quad (12)$$

194 with the empirical proportionality constant $c = 0.01 \text{ m}^{0.5}\text{s}^{0.5}$. This approach ensures a
 195 greatly improved representation of local dispersion compared to the common practice of
 196 considering constant dispersivities even in highly heterogeneous formations. The
 197 spatially variable hydrodynamic self-dispersion coefficients are of critical importance in
 198 the electrostatic cross-coupling between charged species and allow providing a detailed
 199 description of multicomponent ionic transport in heterogeneous formations.

200 The multicomponent transport problem (Eq. 8) is solved numerically on streamline-
 201 oriented grids following the method of Cirpka et al. [61]. The use of such grids,
 202 constructed based on the results of the flow simulation, reduces numerical errors by
 203 minimizing artificial dispersion. The advective-dispersive term is computed with the cell-
 204 centered finite volume method (FVM) [70]. We use a sequential non-iterative operator
 205 splitting approach to decouple the transport and reaction terms. For the advection
 206 problem, we use upwind differentiation for spatial discretization and the explicit Euler
 207 method for time integration. The dispersive fluxes are computed by the implicit Euler
 208 method for integration in time. The resulting system of equations for the dispersion
 209 problem is solved by using the direct matrix solver UMFPACK [71]). In multicomponent
 210 ionic transport problems the system of equations becomes nonlinear due to the
 211 electrostatic interactions between the dispersive fluxes of different charged species.
 212 Therefore, we use an iterative scheme with a Picard loop to linearize the coupled non-
 213 linear set of equations in each temporal step. The detailed computational steps for the
 214 multicomponent transport and reaction calculations are summarized in Table 1.
 215 For each time step, dt , we consider the concentration vector from the advection step (i.e.,
 216 after the advective shift of concentration) as an initial guess of the Picard iteration to
 217 determine the cross-coupled dispersion coefficients (Eqs. 9-10). Afterwards, we
 218 determine the mobility matrix $\mathbf{M}_{\text{MOB},i}^{\text{disp}}$ which results from the spatial discretization on
 219 streamline-oriented grids and contains the divergence of dispersive fluxes defined by the
 220 finite volume method (*Step 2*). The newly computed $\mathbf{D}_{ij}^L, \mathbf{D}_{ij}^T$ and $\mathbf{M}_{\text{MOB},i}^{\text{disp}}$ are then used
 221 to calculate the new concentration vector, $\mathbf{C}_i^{\text{disp}}$ (*Step 3*). Here, $\mathbf{M}_{\text{STORE},i}$ denotes the
 222 storage matrix resulting from the spatial discretization and describes the discrete cell-area

223 of each cell of the domain. C_i^{adv} represents the concentration vector after the advection
 224 step. At each time step, the iteration in the dispersion step repeats until the concentration
 225 vector reaches a constant value: i.e., when the norm of the differences among the
 226 concentration values in two consecutive iterations (κ and $\kappa+1$) converges to a very small
 227 user-defined threshold value (ε).

228 **Table 1:** Algorithm for transient multicomponent ionic transport and reaction
 229 computation.

Discretization:	
$\frac{\partial C_i}{\partial t} + \mathbf{v} \cdot \nabla C_i - \nabla \cdot \left(\sum_{j=1}^N \mathbf{D}_{ij} \nabla C_j \right) \Rightarrow \mathbf{M}_{\text{STORE},i} \frac{\partial C_i}{\partial t} + \mathbf{M}_{\text{MOB},i}^{\text{adv}} C_i + \mathbf{M}_{\text{MOB},i}^{\text{disp}} C_i$	
Advection step:	
$C_i^{\text{adv},t+dt} = C_i^t + (\mathbf{M}_{\text{STORE},i} / dt)^{-1} (-\mathbf{M}_{\text{MOB},i}^{\text{adv},\kappa} C_i^t + \mathbf{b}_i)$	
Dispersion step:	
while $\text{norm}(C_i^{\text{disp},t+dt(\kappa+1)} - C_i^{\text{disp},t+dt(\kappa)}) > \varepsilon$	
Step 1:	Calculate the cross-coupled dispersion coefficients in each cell,
	$\mathbf{D}_{ij}^{L,t+dt(\kappa)} = \delta_{ij} D_{ij}^L - \frac{z_i z_j D_i^L D_j^L C_i^{\text{disp},t+dt(\kappa)}}{\sum_{k=1}^N (z_k^2 D_k^L C_k^{\text{disp},t+dt(\kappa)})}$
	$\mathbf{D}_{ij}^{T,t+dt(\kappa)} = \delta_{ij} D_{ij}^T - \frac{z_i z_j D_i^T D_j^T C_i^{\text{disp},t+dt(\kappa)}}{\sum_{k=1}^N (z_k^2 D_k^T C_k^{\text{disp},t+dt(\kappa)})}$
Step 2:	Calculate mobility matrix for dispersion problem, $\mathbf{M}_{\text{MOB},i}^{\text{disp},t+dt(\kappa)}$
Step 3:	Solve for the concentration,
	$C_i^{\text{disp},t+dt(\kappa)} = (\mathbf{M}_{\text{STORE},i} / dt + \mathbf{M}_{\text{MOB},i}^{\text{disp},t+dt(\kappa)})^{-1} (\mathbf{M}_{\text{STORE},i} C_i^{\text{adv},t+dt} / dt)$
Step 4:	Next iteration: $\kappa = \kappa + 1$
end	
Reaction step:	
$C_i^{\text{disp},t+dt} \rightarrow [\text{PHREEQC}] \rightarrow C_i^{\text{reac},t+dt}$	

230

231

232

3.2 Reaction Calculations and IPhreeqc Coupling

After the advection and dispersion steps, we perform reaction calculations with PHREEQC-3 [18] by using the IPhreeqc module [15]. In our calculations, we use the COM (component object model) version of IPhreeqc which allows all reaction capabilities of PHREEQC to be used by any software and scripting language that can interface with a Microsoft COM server, e.g., Excel®, Visual Basic®, Python, or MATLAB® [14,15]. After updating the species concentration within the transport step, the concentration vector is sequentially passed to IPhreeqc for reaction calculations. In the reaction step, the simulation is performed by considering a batch reactor in each cell of the 2-D model domain that contains user-defined physical and chemical properties representing the reactive processes of interest. After the reaction calculations, the newly updated concentration values in each cell are passed back to the transport model. Besides all dissolved species, the transport calculations also include elemental oxygen (O), hydrogen (H) and charge imbalance (CB) as extra solution components. These parameters allow PHREEQC recognizing the liquid phase (water) and tracking the charge balance which is important in various geochemical calculations [19] as well as for multicomponent ionic transport.

The formulation described above allows performing multicomponent ionic transport calculations in a rigorous way that collectively includes both the electrostatic coupling of dispersive fluxes and the full aqueous speciation computed by PHREEQC.

4. BENCHMARK PROBLEMS

The proposed multicomponent reactive transport model is benchmarked by comparing the model outcomes with: (a) the analytical solution of a 2-D transport problem, (b) a

256 high-resolution experimental dataset, (c) a classical 1-D ion-exchange problem solved
 257 with PHREEQC-3 and (d) 1-D ion exchange considering multicomponent ionic transport.
 258 For the sake of brevity we present in the following sections the benchmark cases (a) and
 259 (d), whereas the examples (b) and (c) can be found in the Supplementary Material.

260 **4.1 Benchmark of Transient Multicomponent Ionic Transport**

261 In order to test the performance of our transient multicomponent ionic transport code in a
 262 two-dimensional flow-through domain, we compare the simulation outcomes with an
 263 analytical solution of the classical 2-D advection-dispersion equation:

$$\frac{\partial C}{\partial t} = -v \frac{\partial C}{\partial x} + D_L \frac{\partial^2 C}{\partial x^2} + D_T \frac{\partial^2 C}{\partial z^2} \quad (13)$$

264 The analytical solution of the advection-dispersion equation in a semi-infinite two-
 265 dimensional perfectly homogeneous domain ($0 < x < \infty$ and $-\infty < z < \infty$), considering transient
 266 transport of a solute initially distributed in a rectangular region with zero influx of solute
 267 mass at the upstream boundary (Eqs. 15-18), is given by [72,73]:

$$\begin{aligned} C(x, z, t) = & \frac{C_0}{4} \left[\operatorname{erfc} \left(\frac{x - x_2 - vt}{\sqrt{4D_i^L t}} \right) - \operatorname{erfc} \left(\frac{x - x_1 - vt}{\sqrt{4D_i^L t}} \right) \right. \\ & \left. + \exp \left(\frac{vx}{D_i^L} \right) \left\{ \operatorname{erfc} \left(\frac{x + x_2 + vt}{\sqrt{4D_i^L t}} \right) - \operatorname{erfc} \left(\frac{x + x_1 + vt}{\sqrt{4D_i^L t}} \right) \right\} \right] \cdot \left[\operatorname{erfc} \left(\frac{z - a}{2\sqrt{D_i^T t}} \right) - \operatorname{erfc} \left(\frac{z + a}{2\sqrt{D_i^T t}} \right) \right] \end{aligned} \quad (14)$$

268 The initial and boundary conditions are defined as:

$$C(x, z, 0) = \begin{cases} C_0 & x_1 < x < x_2 \quad \text{and} \quad -a < z < a \\ 0 & \text{otherwise} \end{cases} \quad (15)$$

$$vC|_{x=0^+} = 0 \quad (16)$$

$$\frac{\partial C}{\partial x}(\infty, z, t) = 0 \quad (17)$$

$$\frac{\partial C}{\partial z}(x, \pm\infty, t) = 0 \quad (18)$$

269 where x_1 and x_2 are the longitudinal positions delimiting the initial location of the solute
 270 source. In the transverse direction, the solute is initially located between $-a$ and a .

271 We consider a two-dimensional homogeneous domain of $100 \text{ cm} \times 12 \text{ cm}$, which is
 272 discretized into 100 ($\Delta x = 1 \text{ cm}$) and 240 ($\Delta z = 0.5 \text{ mm}$) cells along the longitudinal and
 273 transverse dimension, respectively. The transport simulations are run for a total
 274 simulation time of $t = 18$ hours with a uniform horizontal velocity of $v = 1.0 \text{ m/day}$. The
 275 porosity of the flow-through system is 0.41. We consider a rectangular solute source,
 276 with dimensions of $2 \text{ cm} \times 2 \text{ cm}$, initially located 2 cm downstream of the inlet boundary,
 277 between 5 and 7 cm along the vertical dimension (Fig. 2).

278 The simulation is performed for the transport of a single 1:1 electrolyte (NaCl) in pure
 279 ambient water. In such ionic systems, the electrostatic interactions couple the movement
 280 of the cation (Na^+) and the anion (Cl^-) and lead to an identical displacement of the two
 281 species. As a result, although the strong electrolyte (NaCl) fully ionizes in the aqueous
 282 solution and the two ions (Na^+ and Cl^-) are characterized by different mobility, they

283 travel as a single species in order to maintain electroneutrality. Hence, for this particular
 284 case, the diffusion (and dispersion) of these two ions can be characterized by a single
 285 diffusion coefficient (e.g., [36]):

$$D_{NaCl} = \frac{|z_{Na^+}| + |z_{Cl^-}|}{|z_{Na^+}|/D_{Cl^-}^{aq} + |z_{Cl^-}|/D_{Na^+}^{aq}} \quad (19)$$

286 where D_{NaCl} represents the combined diffusion coefficient of the electrolyte. z_{Na^+} , z_{Cl^-}
 287 and $D_{H^+}^{aq}$, $D_{Cl^-}^{aq}$ are the charge and the aqueous diffusion coefficients of Na^+ and Cl^- ,
 288 respectively. Self-diffusion coefficients of sodium and chloride as well as of other ions
 289 used in the following sections are reported in Table 2. The value obtained combining
 290 diffusion coefficients of Na^+ and Cl^- (Eq. 19) for the salt is $D_{NaCl} = 1.44 \times 10^{-9} \text{ m}^2/\text{s}$.
 291 Therefore, the electrostatic ionic interactions reduce the multicomponent ionic transport
 292 problem into a single-species conservative transport problem. Thus, for this special case,
 293 the outcomes of the 2-D transient multicomponent ionic transport model can be directly
 294 compared with the results of the analytical solution (Eq. 14). In order to simulate
 295 transport in flow-through systems the hydrodynamic dispersion coefficients (Eq. 11) are
 296 calculated using the combined salt diffusion coefficient (Eq. 19) for the analytical
 297 solution (Eq. 14) and the self-diffusion coefficients of the individual ions for the
 298 numerical model. The latter takes into account the electrostatic interactions between Na^+
 299 and Cl^- in the pore water by coupling their dispersive fluxes as explained in Section 2 and
 300 Section 3.

301 The comparison between the multicomponent ionic transport model and the analytical
 302 solution at the end of $t = 18$ hours of simulation is shown in Fig. 2. The instantaneous

rectangular slug source spreads and approaches a Gaussian elliptical shape during the transport through the homogeneous porous medium (Fig. 2a-c). It is evident from the two-dimensional concentration distributions that the concentrations both from the multicomponent ionic transport simulations (Fig. 2a-b) and from the analytical solution (Eq. 14, Fig. 2c) are very similar. Fig. 2 also shows the longitudinal (panel d) and transverse (panel e) concentration profiles along the longitudinal and transverse axes through the center of the plume. The coupled displacement of the Na^+ and Cl^- ions results in overlapping concentration of these species both in the longitudinal and in the transverse direction. These profiles perfectly match with the concentration profiles of the combined electrolyte (i.e., NaCl salt as a single uncharged species) computed with the analytical solution. Thus, these results validate the accuracy of the transient multicomponent ionic transport simulations in conservative two-dimensional systems.

Table 2: Aqueous diffusion coefficients of different ions.

Diffusion coefficients	$D^{aq} [\text{m}^2/\text{s}]^a$
H^+	8.65×10^{-9}
Mg^{2+}	0.63×10^{-9}
Cl^-	1.81×10^{-9}
Na^+	1.20×10^{-9}
Br^-	1.86×10^{-9}
K^+	1.77×10^{-9}
Ca^{2+}	0.71×10^{-9}
NO_3^-	1.70×10^{-9}

^a values from Lasaga [74], corrected for temperature and viscosity changes at 20°C

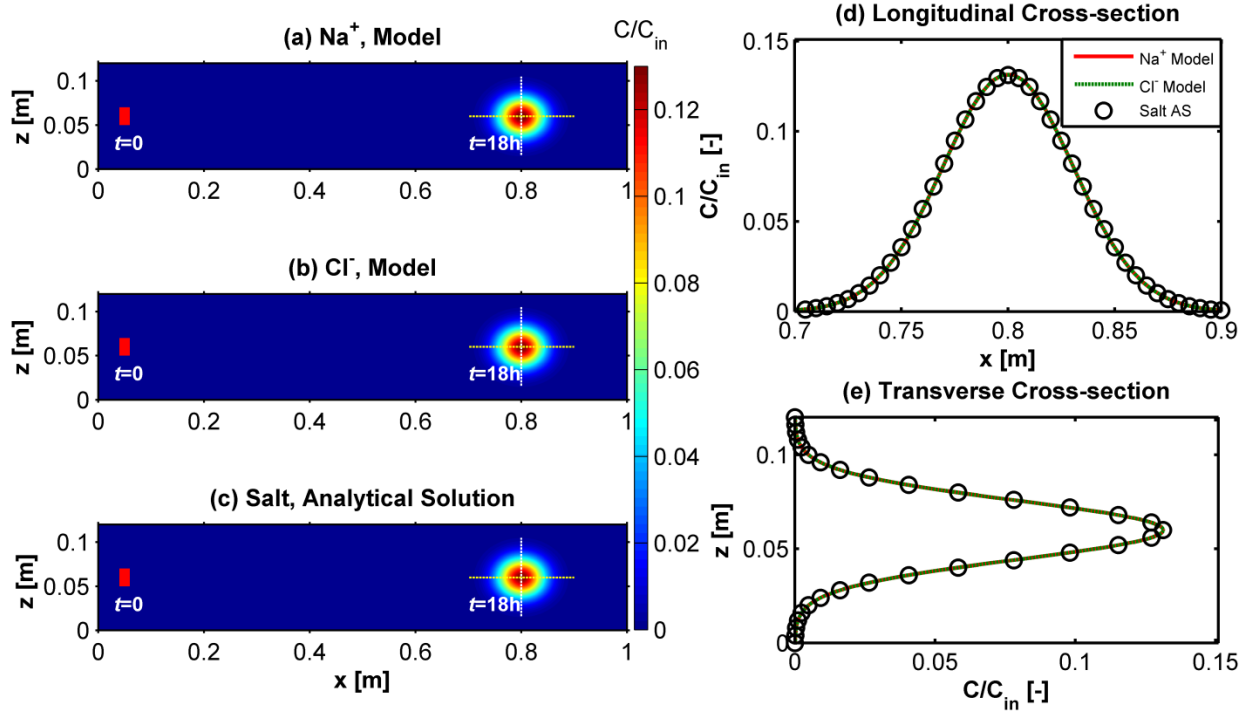


Figure 2: Comparison of the multicomponent ionic transport model and 2-D analytical solution for the transport of NaCl in pure water at $v = 1$ m/day: 2-D concentration distributions after $t = 18$ hours (a-c); longitudinal cross sectional profiles at $z = 6$ cm (d); transverse cross sectional profiles at $x = 80$ cm (e).

4.2 Benchmark of IPhreeqc Coupling: Ion-Exchange with Multicomponent Ionic Transport and Charge Interactions

In order to validate the coupling of our transport code with the geochemical code PHREEQC, we consider the example problem 11 of the PHREEQC-3 manual [18]. This example includes the advective-dispersive transport of ionic species in a one-dimensional, 8 cm long column containing a cation exchanger. The exchanger column, initially in equilibrium with a solution containing Na⁺, K⁺ and NO₃⁻, is continuously flushed with a CaCl₂ solution. As a consequence, the cations (Na⁺, K⁺ and Ca²⁺) undergo ion-exchange reactions with the exchanger and new equilibrium compositions of the exchanger and the pore water are established. The comparison between the 1D

PHREEQC simulation and the 2D simulation carried out with the proposed code is presented in the Supplementary Material. The ion-exchange problem was also extended to the case of transient multicomponent ionic transport. In this example, we specifically focus on multicomponent diffusion (with charge effects) and ion-exchange problem. In order to focus on the multicomponent effects, we consider diffusion-dominated transport in the virtual column setup, by decreasing of a factor of ten the value of the seepage velocity ($v = 0.024$ m/day). The column geometry, the exchanger properties and the involved ions and concentrations are kept the same as in the original example described above. Instead of a single diffusion coefficient for all ionic species, species-specific aqueous diffusion coefficients are used for different ions. The self-diffusion coefficients used for different species are reported in Table 2. For the sake of simplicity, dispersivity is neglected and thus is set to zero and the pore diffusion coefficients are assumed to be identical to the aqueous diffusion coefficients (i.e., porosity, $\theta = 1$). The 1-D PHREEQC simulations are conducted by using the keyword **multi_d**, which allows accounting for multicomponent ionic transport [29]. On the other hand, in our two-dimensional transport code coupled with PHREEQC, multicomponent ionic transport calculations are performed by solving Eqs. (7-10) as illustrated in Section 3 and Table 1. Fig. 3 represents the simulated effluent breakthrough curves of different ionic species. Notice that, due to a smaller advective velocity, diffusion becomes more dominant in this case compared to the advection-dominated ion-exchange problem (Fig. S5, Supplementary Material). This is reflected in the smoother temporal concentration profiles of the ionic species. The evolution of Cl^- front shows an interesting pattern, with a sudden increase of Cl^- concentration, after ~ 1.75 PV when Ca^{2+} breakthrough starts. Such behavior is due to the

multicomponent ionic transport through the exchanger column and the requirement of maintaining charge balance throughout the domain. Furthermore, the two simulations, using PHREEQC alone in a 1-D domain and using the 2-D multicomponent ionic transport code combined with PHREEQC in a uniform 2-D domain (equivalent to 1-D), have the same outcome which, therefore, validates the transient multicomponent ionic transport calculations coupled with chemical reactions.

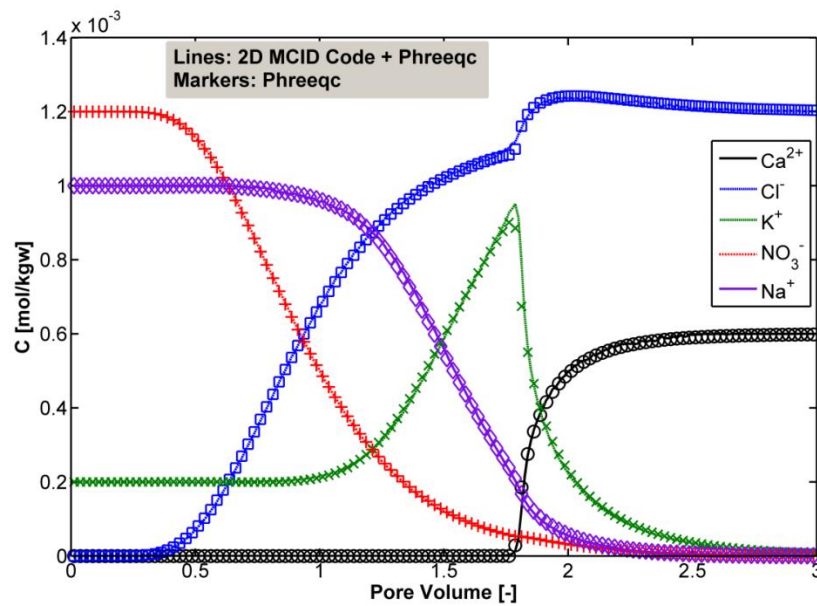


Figure 3: Benchmark of IPhreeqc coupling with the 2-D transport code for an example of ion-exchange coupled to multicomponent ionic transport with electrochemical migration.

5. EXAMPLES OF MULTICOMPONENT IONIC TRANSPORT SIMULATIONS

In this section we present scenarios of multicomponent transport of ionic solutes in both homogeneous and heterogeneous domains. Section 5.1 focuses on conservative multicomponent transport of electrolyte systems. The impact of charge effects on breakthrough curves and plume dilution of the different ionic species during conservative

transport are analyzed. Section 5.2 illustrates multicomponent transport of charged species undergoing ion-exchange reactions. We present scenarios with increasing level of complexity in terms of physical heterogeneity (i.e., spatially variable hydraulic conductivity) and chemical heterogeneity (i.e., spatially variable ion-exchange capacity).

5.1 Conservative Transport

5.1.1 Simulations in Homogeneous Domain

The simulations were performed to show the influence of charge interactions on transient multicomponent ionic transport. We consider two different domains, a homogeneous porous medium and a heterogeneous formation, at two different scales. For the homogeneous case, we select a 2-D domain with dimensions of $100\text{ cm} \times 20\text{ cm}$ ($L \times W$), similar to the laboratory setup recently used to investigate multicomponent ionic transport [37-39], and with a uniform distribution of hydraulic conductivity and flow-velocity. Such simulation domain is representative of typical laboratory bench-scale quasi two-dimensional flow-through chambers packed with uniform grain sized material (e.g., [39,43,75]). The simulations were run, by considering a rectangular slug of electrolytes as initial condition, at two different horizontal flow velocities of 0.1 m/day and 1.0 m/day . At each flow velocity, three different combinations of electrolyte scenarios are considered: (i) transport of a single electrolyte (HCl) in pure water; (ii) transport of a single electrolyte (HCl) in a background electrolyte solution (NaBr); and (iii) transport of mixed electrolytes (H^+ , Mg^{2+} and Cl^-) in pure water. The selection of this particular set of electrolytes is based on the variability of their aqueous diffusion coefficients (Table 2) and demonstrates the multicomponent charge coupling effects on ions undergoing conservative transport. The geometry, hydraulic and transport properties of different

simulation domains are summarized in Table 3. It should be noted that these simulations are run by considering the assumption that the transported ionic species do not interact with the solid matrix and perfect conservative conditions exist.

Fig. 4 summarizes the breakthrough curves and transient flux-related dilution index for different electrolyte cases at the outlet end of the homogeneous meter-scale domain. The flux-related dilution index is a metric of mixing, originally developed for steady-state plumes [76], that expresses dilution as the act of distributing a given solute mass flux over a larger water flux and determines an effective volumetric discharge transporting the solute flux at a given longitudinal cross section. For the transient multicomponent transport of ionic species in flow-through domains, the flux-related dilution index of an ion “ i ” can be defined as [77]:

$$E_{Q,i}(x,t) = \exp \left(- \int_{\Omega} p_{Q,i}(x,t) \ln p_{Q,i}(x,t) q_x(x,t) d\Omega \right) \quad (20)$$

where $q_x = v\theta$ is the longitudinal component of specific discharge, Ω is the cross-sectional area, θ is the porosity, and $p_{Q,i}$ is the flux-related probability density function of the charged species “ i ” at time t :

$$p_{Q,i}(x,t) = \frac{C_i(x,t)}{\int_{\Omega} C_i(x,t) q_x(x,t)} \quad (21)$$

The simulation outcomes at velocity of 0.1 m/day and 1 m/day are shown in Figs. 4a-f and 4g-l, respectively. For the transport of a single electrolyte (HCl) in pure water, despite having very different diffusivities (Table 2), the breakthrough curves of the cation (H^+) and anion (Cl^-) are identical at both flow velocities (Fig. 4a and 4g). On the other

412 hand, during transport in the presence of a background electrolyte, their breakthrough
413 profiles are significantly different, with the faster ion (H^+) having more spread profiles
414 and lower peak concentrations compared to the slower one (Cl^-) (Fig. 4b and 4h). The
415 profiles of flux-related dilution index show identical values for transport in pure water
416 (Fig. 4d and 4j); whereas in the case of background electrolyte the cation (H^+) plume is
417 considerably more diluted (approximately 2 times) than the anion (Cl^-) plume (Fig. 4e
418 and 4k). This behavior is induced by the charge interactions between positively and
419 negatively charged species. During transport in pure water the cation and anion travel
420 together in order to fulfill the local charge balance and thus they are electrostatically
421 coupled. On the other hand, when the same ions are transported through a background
422 electrolyte solution, the domain is locally charge balanced by the background ions and,
423 consequently, the cation and anion in the solute plume can travel and subsequently dilute
424 according to their self-diffusive/dispersive properties. However, in both cases the $E_{Q,i}$
425 profiles for different ions show a monotonic increase over time at the outlet cross-section
426 of the domain (Fig. 4e and 4f).

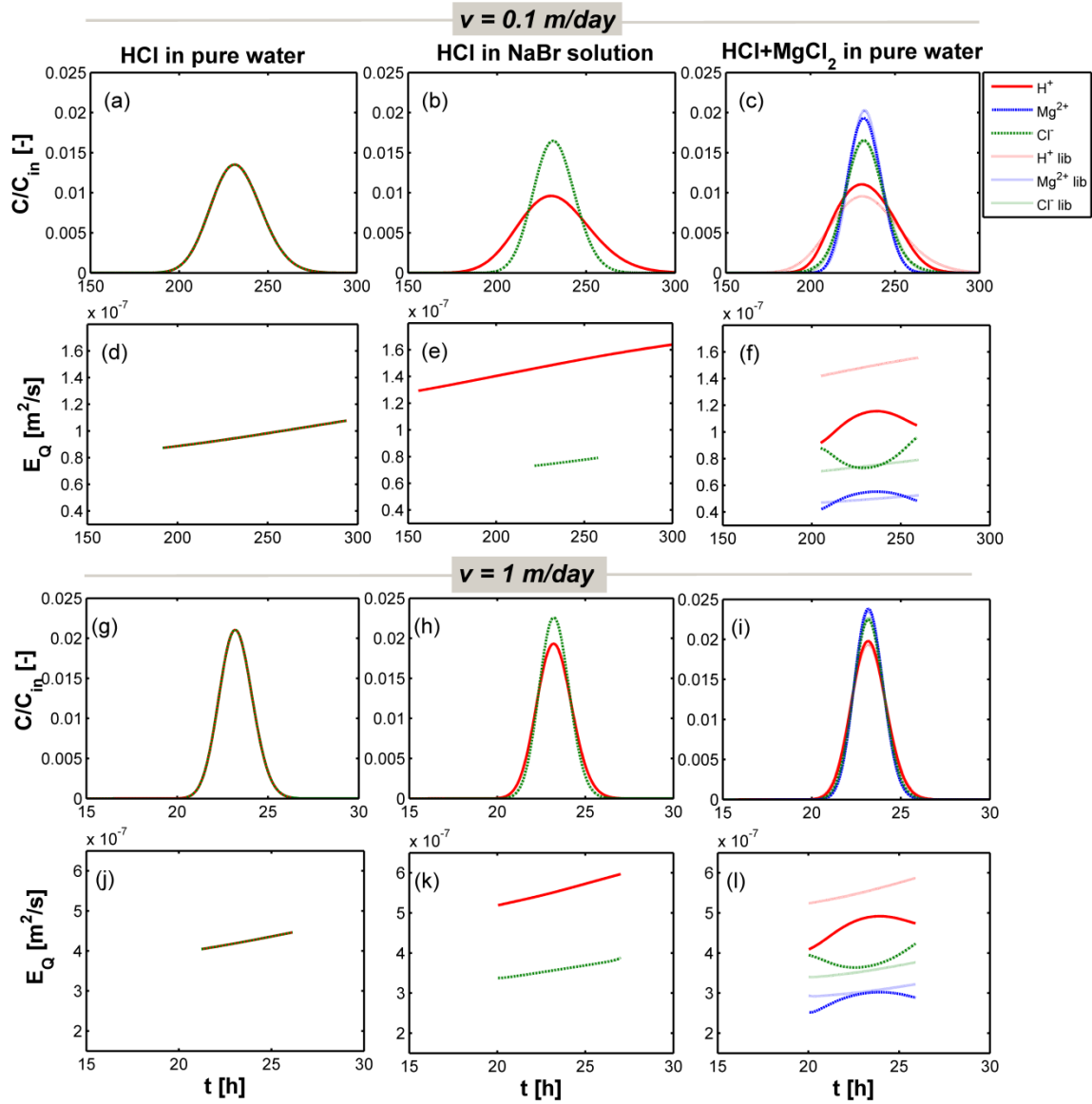


Figure 4: Breakthrough curves (a-c and g-i) and flux-related dilution indices (d-f and j-l) for simulations at $v = 0.1$ m/day (a-f) and $v = 1$ m/day (g-l) in a homogeneous domain. $E_{Q,i}$ values are calculated for a concentration threshold equal to 10^{-6} of the peak concentration for each species.

For the transport of mixed electrolytes in pure water (H⁺, Mg²⁺ and Cl⁻), the breakthrough curves show a distinct pattern which follows the same order as suggested by their self-diffusivities (Table 2): where H⁺ has the most spread profile with the lowest peak concentration and Mg²⁺ shows the least spread profile and the highest peak concentration (Fig. 4c). The Cl⁻ profile lies in between those of the cations. Due to the electrostatic

437 interaction during the displacement of the different ions, the profiles are also different
 438 compared to those of transport under “liberated” conditions (i.e., when they are
 439 transported as uncharged species). The behavior of the flux-related dilution index profiles
 440 of the ionic species for this scenario is quite interesting. The cation dilution profiles show
 441 a bulge-shape resembling a concave function. The cations have an increasing pattern of
 442 dilution reaching a maximum, and afterwards decreasing again (red and blue solid lines;
 443 Fig. 4f). The pattern is opposite (convex shaped) for the anion (Cl^-) for which the E_Q
 444 profile decreases and reaches a minimum at around mean breakthrough time and
 445 afterwards it starts increasing again (green lines; Fig. 4f). Such dilution behavior is
 446 significantly different compared to the monotonic increase at their “liberated” state
 447 (dotted lines; Fig. 4f) and can be explained considering the ionic interactions between the
 448 transported species. In fact, at early breakthrough times, when the fringe of the plume
 449 arrives at the outlet boundary, H^+ is more enriched compared to Mg^{2+} because of the
 450 higher diffusive/dispersive properties of H^+ . As a consequence, H^+ is mainly responsible
 451 for counterbalancing the negative charge of Cl^- in the fringe area. Therefore, at the edge
 452 of the plume, the dilution of H^+ and Cl^- are similar, as reflected in their very early and
 453 late time $E_{Q,i}$ values, and these ions tend to be electrostatically coupled. Thus, among
 454 these two abundant species in the fringe zone, the diffusivity of H^+ decreases and the one
 455 of Cl^- increases compared to their true “liberated states” in order to maintain charge
 456 balance. On the other hand, in the center of the plume, Mg^{2+} has a higher relative
 457 concentration and hence higher contribution to counter the negative charge of Cl^- . So, in
 458 this case, E_{Q,Cl^-} decreases due to a stronger coupling to a slower positive ion (Mg^{2+}), and
 459 for the same reason Mg^{2+} dilution increases compared to its liberated values (Fig. 4f).

The differences between the actual dilution of the ions' plumes compared to their theoretical displacements at "liberated state" are notable for all the reported ions, as shown by the different patterns of the corresponding lines in Fig. 4f.

Similar patterns of concentration and dilution breakthrough curves are obtained at higher velocity ($v = 1$ m/day) (Figs. 4g-l). Due to the advection-dominated transport, breakthrough curves are less spread (narrow profiles with higher peak concentrations) compared to their respective cases at slow velocity ($v = 0.1$ m/day). Interestingly, because of the higher Péclet numbers (i.e., higher values of dispersion coefficients) at $v = 1$ m/day the absolute values of dilution indices ($E_{Q,i}$) are considerably higher (approximately 5 times) with respect to the ones obtained at slow velocity (Figs. 4j-l, 4d-f). This implies that, even though the breakthrough curves and the concentration distribution are less spread, the plumes are in fact more diluted at higher seepage velocity, since the mass fluxes of the different ions are distributed over larger water fluxes.

5.1.2 Simulations in Heterogeneous Domain

The analogous set of simulations was also performed in a heterogeneous domain to investigate the large-scale effects and the influence of heterogeneity on breakthrough and dilution during conservative multicomponent ionic transport. The simulations were run in a randomly generated two-dimensional flow-field ($20 \text{ m} \times 2.5 \text{ m}$) representing a vertical cross-section of a mildly heterogeneous aquifer. The hydraulic conductivity statistics are consistent with those reported for the Borden aquifer [78] and the mean hydraulic gradient was adjusted to produce average flow velocities of 0.1 and 1 m/day. The domain is discretized into 200 cells ($\Delta x = 10 \text{ cm}$) in the horizontal direction and 250 cells ($\Delta z = 1 \text{ cm}$) in the vertical direction. The heterogeneous conductivity field is generated with an

exponential covariance model and by using the spectral approach described by Dykaar and Kitanidis [79]. The summary of hydraulic and transport parameters used in the simulations are given in Table 3.

Table 3. Summary of geometry, flow and transport parameters of the homogeneous and heterogeneous domains.

Parameters	Homogeneous ^a	Heterogeneous ^b
Domain size (L×H) [m]	1 × 0.2	20 × 2.5
Discretization, $\Delta x/\Delta z$ [cm]	0.5/0.1	10/1
Slug size [m]	0.02 × 0.02	0.4 × 0.2
Average hydraulic conductivity [m/s]	1.27×10 ⁻²	9.75×10 ⁻⁵
$\sigma^2_{\ln K}$	-	0.29
Average horizontal flow velocity [m/day]	0.1; 1	0.1; 1
Average porosity [-]	0.41	0.34

^aData consistent with the experimental setup of Rolle et al. [37]

^bData consistent with the characterization of the Borden aquifer (Sudicky [78])

Fig. 5 shows the results of conservative transport simulation of mixed electrolytes in the generated 2-D random fields for an average flow velocity of 1 m/day, using spatially-variable local hydrodynamic dispersion coefficients in which the mechanical dispersion term is linked to the hydraulic conductivity through the average grain size (Eq. 12). The simulated velocities and streamlines are shown in Fig. 5a. The concentration distribution of the plume containing mixed electrolytes (HCl and MgCl₂) after 7 days of simulation is depicted in Fig. 5b-d. It is evident that due to heterogeneity and flow variability, the shapes of the different ionic plumes are irregular. It is interesting to notice that even in this spatially variable domain and under an advection-dominated regime (average $v = 1$ m/day), the compound-specific behavior of the different ions is still significant as shown by the different distributions of the two cations and of the anion concentration. Due to a higher diffusive/dispersive properties, the H⁺ plume is evidently more diluted and

shows a lower peak concentration compared to the other two ions (Fig. 5b). On the other hand, the Mg^{2+} plume is more affected by the spatial variability of the velocity distribution and consequently results in a more stretched but less diluted plume with a higher peak concentration (Fig. 5c). The shape of the anion (Cl^-) plume appears to be in between those of the cations.

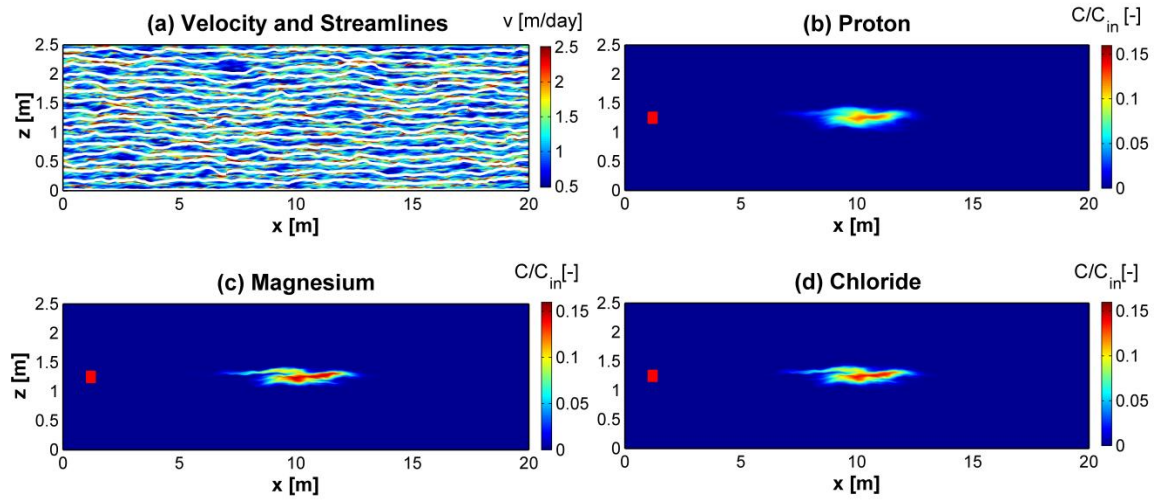


Figure 5: Seepage velocity distribution and streamlines (a); 2-D concentration maps (b-d) for mixed electrolyte case at $v = 1$ m/day after $t = 7$ days. The red rectangle represents the initial location of the solute slug (b-d).

The breakthrough curves of concentration and flux-related dilution index ($E_{Q,i}$), at the end of the domain, are illustrated in Fig. 6 for different simulations. Although the shape of the 2-D concentration distribution for different ions looks very irregular (non-Gaussian; Figs. 5b-d), their depth-integrated breakthrough curves have almost regular shape (Figs. 6a-c, g-i) in this mildly-heterogeneous domain.

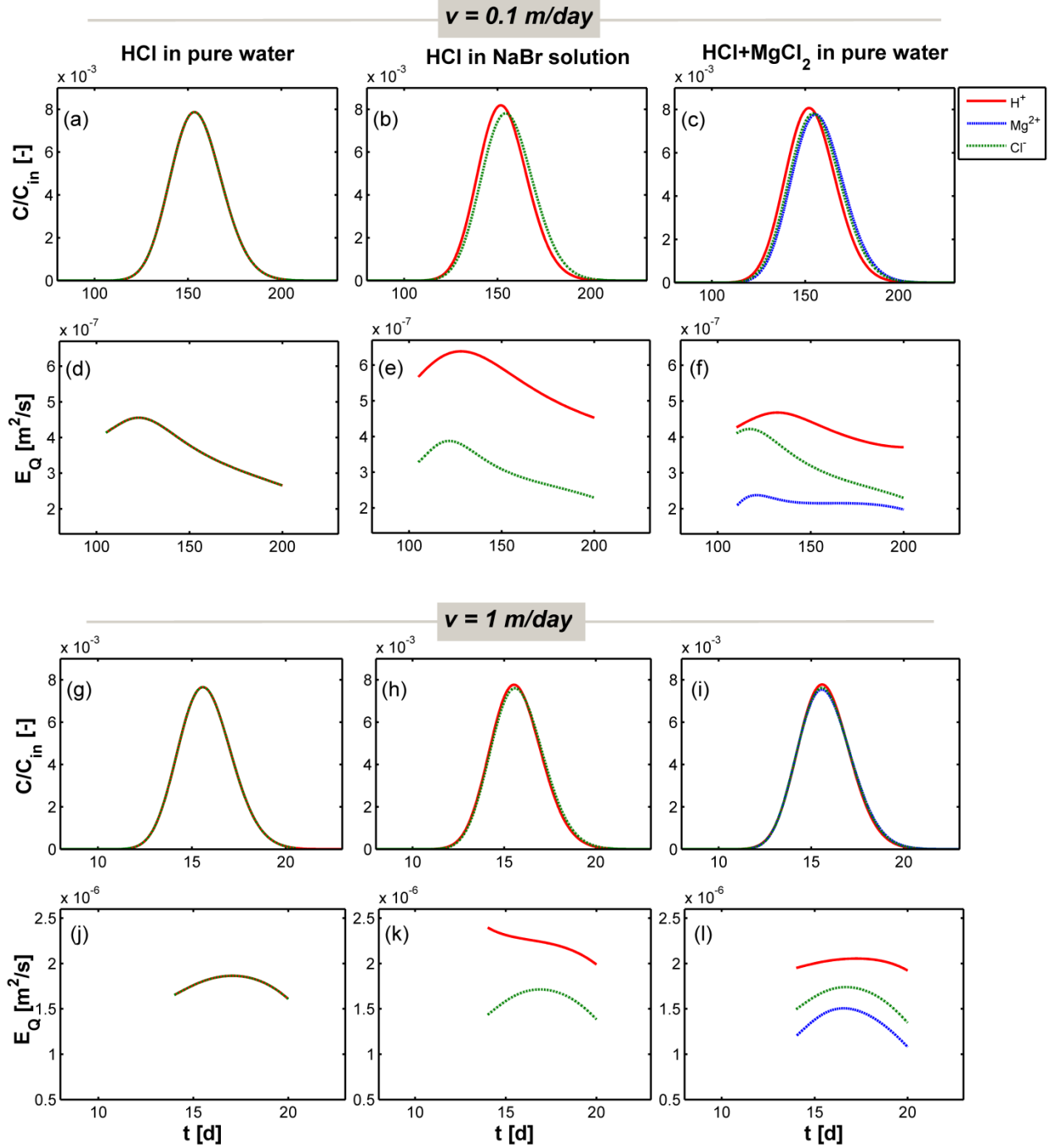


Figure 6: Breakthrough curves (a-c and g-i) and flux-related dilution indices (d-f and j-l) for simulations at $v = 0.1 \text{ m/day}$ (a-f) and 1 m/day (g-l) in a heterogeneous domain. $E_{Q,i}$ values are calculated for a concentration threshold equal to 10^{-6} of the peak concentration for each species.

For the transport of both HCl in a background electrolyte (Fig. 6b,h) as well as for the case of mixed electrolyte in pure water (Fig. 6c,i), the differences among the ionic temporal profiles are smaller compared to those observed in homogeneous domain. However, the differences in dilution between the ions are still significant as shown by the computed trends of $E_{Q,i}$. Unlike the regular increase of $E_{Q,i}$ in the homogeneous domain, the dilution breakthroughs in the heterogeneous flow field have a non-monotonic pattern. As observed in pore-scale domains [77], also for these continuum simulations such behavior can be attributed to the spatial variability of the velocity field and mass transfer limitations in the low-permeability zones of the heterogeneous flow field. Despite the different and irregular shape of the dilution breakthroughs compared to a homogeneous domain, the computed values of $E_{Q,i}$ at both flow velocities show the clear and persistent effect of the electrostatic coupling also in the heterogeneous flow field. This important feature can also be clearly appreciated from the maps of the ion concentration distributions (Fig. 5) but would be missed if one were to analyze exclusively flux-averaged concentration breakthrough curves at the outlet of the domain (Fig. 6 a-c and g-i).

The effect of electrostatic coupling is also evident from the maps of the dispersive flux components. As an example, Fig. 7 shows the results of transverse dispersive fluxes for the case of mixed electrolytes at $v = 0.1$ m/day. It is interesting to notice the interplay between the pure dispersive and the electrochemical migration components. For instance, considering H^+ it can be clearly observed that the electromigration component can have both a positive and a negative contribution to the total dispersive flux (Fig. 7g). Thus, the displacement of the ion can be increased or decreased in different locations within the

plume. Similar considerations are valid for the other cation and for the anion. The latter shows an inversely correlated behavior with respect to H^+ , with displacement of Cl^- ions enhanced in the plume fringe, where they are mostly coupled to H^+ , and decreased in the plume core, where the charge interaction is stronger with Mg^{2+} . Mapping of the ionic flux components helps understanding and visualizing the coupling between the transport of charged species and confirms a similar behavior as noticed in the small scale homogeneous domain by analyzing the dilution breakthrough curves (Fig. 4f and 4l).

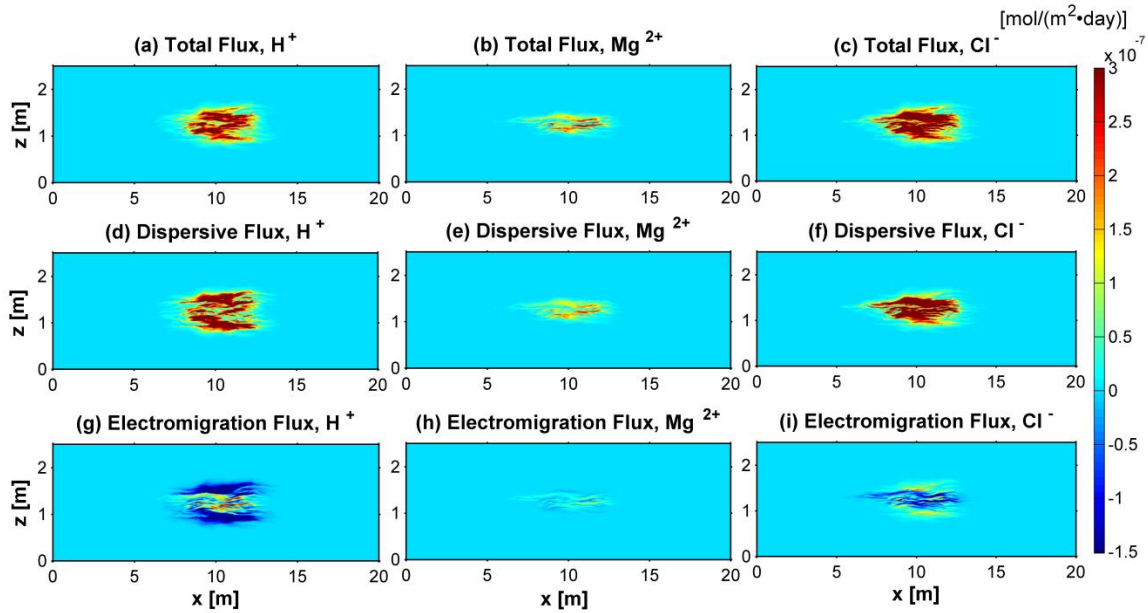


Figure 7: Maps of multicomponent ionic transverse fluxes for the transport of mixed electrolytes after 70 days ($v = 0.1$ m/day): Total fluxes (a, b, c), Dispersive fluxes (d, e, f) and Electrochemical migration fluxes (g, h, i). The direction from the core to the fringe of the plume is considered positive for the calculated fluxes.

5.2 Multicomponent Reactive Transport

In this section we present examples of two-dimensional multicomponent ionic transport coupled to chemical reactions in physically and chemically heterogeneous domains. We consider ion-exchange reactions and, similarly to a previous study [80], we extend a 1-D

example problem (Section 4.2) to two-dimensional spatially-variable domains. We focus on multicomponent ionic transport and we consider a slug release of CaCl_2 in a 2-D domain containing Na^+ , K^+ and NO_3^- as initial and ambient solution. The simulations are run in heterogeneous domains with different distributions of key physical and chemical parameter such as the hydraulic conductivity and the cation exchange capacity (Table 4).

Table 4: Description of the multicomponent reactive transport scenarios.

Scenario	<i>K</i> distribution	<i>CEC</i> distribution	Domain size	Slug size
A	heterogeneous	homogeneous	20 m \times 2.5 m	4 m \times 0.3 m
B	heterogeneous	heterogeneous	20 m \times 2.5 m	4 m \times 0.3 m

The simulations were run in the randomly generated 2-D fields with the same geometry and hydraulic properties of those used in Section 5.1.2. Fig. 8 shows distributions of the controlling physical and chemical parameters. In both scenarios, we consider solute slugs of CaCl_2 (6 mM), initially placed 1 m downstream of the inflow boundary and with dimensions of 4 m \times 0.3 m, that were transported through the heterogeneous domains.

The inflow and initial solutions contain NaNO_3 (1 mM) and KNO_3 (0.2 mM).

Scenario A considers the effects of physical heterogeneity on the reactive transport problem. In this particular scenario, a uniform value of *CEC* (1.1 meq/L; same as [18]) was used throughout the entire physically heterogeneous domain.

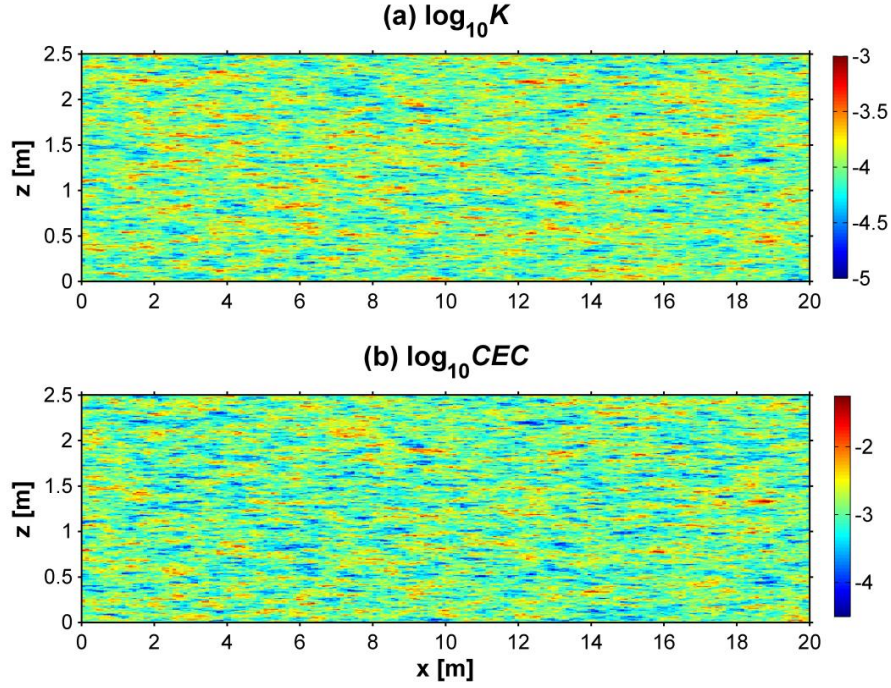


Figure 8: (a) Spatial distribution of hydraulic conductivity K (m/s) used in the simulated reactive transport scenarios A and B. (b) Spatial distribution of cation exchange capacity, CEC (eq/L) used in Scenario B.

In Scenario B, CEC values (Fig. 8b) were attributed to each cell of the domain considering a negative correlation with hydraulic conductivity as suggested in previous studies (e.g., [80-83]):

$$\ln CEC = a \ln K + b \quad (22)$$

where a and b are coefficients relating the hydraulic conductivity, K and the cation exchange capacity, CEC . In a field study, Christiansen et al. [81] identified a negative correlation between K and CEC in an aquifer ($a = -0.59$) composed of calcareous and non-calcareous layers. We base our simulations on the negative correlation proposed in that study, implying that the low-permeability regions have higher cation exchange capacity than the high-permeability zones (and vice versa).

Fig. 9 summarizes the results of the multicomponent reactive transport simulations performed in scenarios A and B. The top row of panels depict the 2-D concentration distribution of the cation plumes (Ca^{2+} ; Fig. 9a,e) and the lower two rows of panels show the distribution of the background cations (Na^+ and K^+) after 75 days of simulation. All simulations are run at an average seepage velocity of 0.1 m/day. Fig. 9a-c shows the spatial distribution of different cations plumes in Scenario A. In this domain, the solute slug CaCl_2 moves with groundwater along the 2-D random flow-field containing homogeneous cation-exchange properties. All the ionic plumes show irregularities because of the spatially variable hydraulic conductivity and velocity distributions. The displacing cation, Ca^{2+} , shows a tailing in the upstream front and a sharper interface in the downstream front of the plume. As it propagates through the domain, Ca^{2+} reacts with the exchanger and displaces the background cations (K^+ and Na^+) from the solid. Because of different affinities towards the solid phase, a chromatographic sequence is clearly observed among the positive ions: with Na^+ (lowest affinity, Fig. 9c) being the first species released from the solid phase, followed by K^+ (Fig. 9b) and, finally, by the displacing species Ca^{2+} (highest affinity, Fig. 9a).

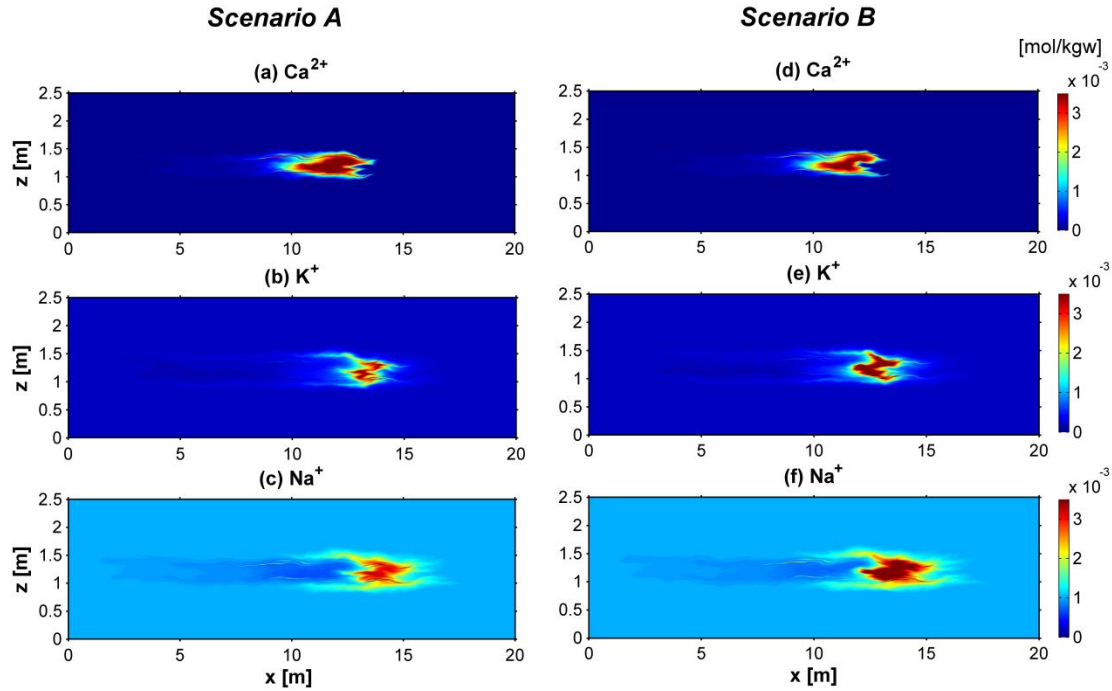


Figure 9: 2-D concentration distribution of cations in Scenario A (a-c) and B (d-f) after 75 days of simulation.

The effect of K^+ and Na^+ displacement from the solids is also reflected from the fact that these background cations show a surplus of dissolved concentration relative to their initial values (Fig. 9b-c). The center of mass of the cation plumes also moves with different apparent velocities: with Na^+ being the fastest species and Ca^{2+} being the slowest one.

In Scenario B, the solute slug migrates with groundwater along random flow paths and in a geochemically heterogeneous domain. The concentration and spreading of cation plumes (Fig. 9d-f) are quite different compared to the previous scenario. The background ions (K^+ and Na^+) contain relatively higher concentration in the dissolved phase compared to Scenario A (relative differences in the peak concentrations are $\sim 32\%$ for K^+ and $\sim 11\%$ for Na^+). Conversely, Ca^{2+} shows a distribution that has smaller peak concentration (approximately 22%) relative to the plume in Scenario A (Fig. 9a,d). This

implies that the heterogeneous distribution of geochemical properties leads to an enhancement of ion-exchange reactions and more effective retention of Ca^{2+} . After 75 days of simulation, the total mass of Ca^{2+} in the dissolved phase is ~34% smaller in the chemically heterogeneous domain with respect to Scenario A. This behavior can also be further confirmed from the depth-integrated breakthrough curves of Ca^{2+} at the end of the heterogeneous domains (Fig. 10a). The depth-integrated peak concentration of Ca^{2+} in Scenario B (red solid line) is significantly smaller (approximately ~5 times) compared to Scenario A (black solid line). The mean arrival of breakthrough in Scenario B is also considerably delayed (~20 days) compared to Scenario A. The dotted lines represent the breakthrough curves of respective scenarios by ignoring the charge interactions (i.e., as “liberated state”); while keeping the other hydraulic, transport and geochemical conditions identical in the simulations. Scenario B is a random realization with the same average CEC of scenario A. However, the total cation exchange capacity in the two systems is different and this has an important effect on the breakthrough of calcium in the two setups. Therefore, we considered an additional case in which not the average, but the total CEC is the same in the two cases. The results of this additional simulation are reported in Fig. 10b and show a closer behavior in terms of both arrival time and peak concentration between scenario A and scenario B. It is interesting to notice that in all cases a contribution due to electrochemical migration can be appreciated even in the integrated profiles. Such contribution, in the considered physically and/or chemically heterogeneous realizations, tends to cause an additional retardation of the calcium plumes. We attribute this observation to the enhancement of Ca^{2+} dispersion fluxes through the electrostatic coupling with the more mobile anions present in the domain.

This results in lower peak concentrations and more spread Ca^{2+} profiles. Such differences in displacement do not only influence the breakthrough of calcium but also the mass recovered at the outlet. In fact, the electromigration contribution to the dispersive fluxes causes enhanced displacement of calcium at the outer fringe of the plume. In these regions calcium comes into contact with solid with available CEC and, thus, it is retained more effectively in the solid phase. As a consequence, a lower portion of the mass is recovered at the outlet.

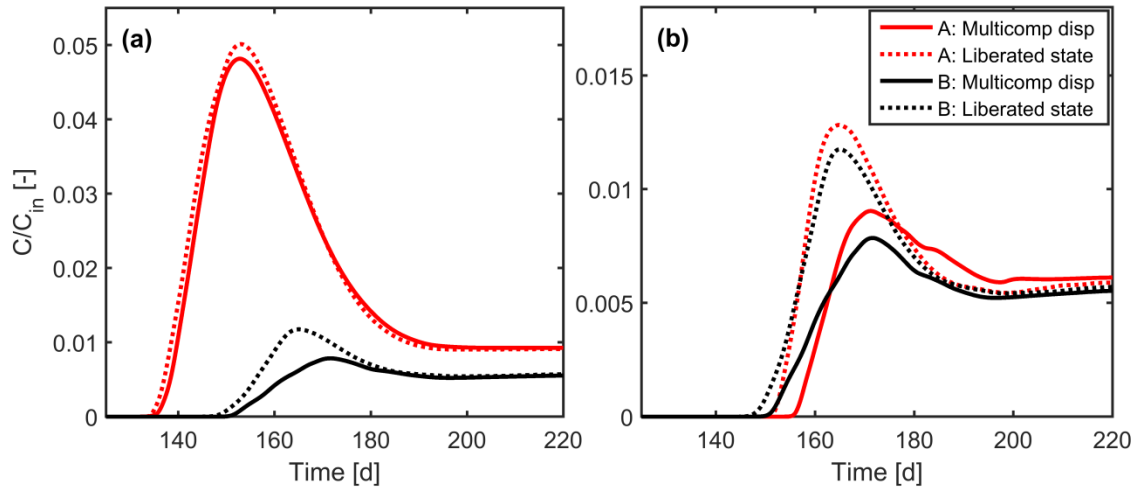


Figure 10: Depth-integrated breakthrough curves of Ca^{2+} at the end of the heterogeneous domain in Scenario A and B, considering multicomponent ionic transport (solid lines) as well as transport in “liberated” state (dotted lines). (a) Simulations with same average CEC between Scenario A and B; (b) Simulations with same total CEC between Scenario A and B.

6. SUMMARY AND CONCLUSIONS

In this paper, we presented a two-dimensional multicomponent reactive transport model which is capable of taking into account the electrochemical migration effects during ionic transport as well as a wide range of geochemical reactions. The modeling framework is based on a multicomponent formulation of diffusive/dispersive fluxes and on the

compound-specific and spatially variable description of local hydrodynamic dispersion. The proposed approach allows a detailed description of physical and electrochemical processes during multicomponent ionic transport in both homogeneous and heterogeneous formations. Additionally, the multicomponent ionic transport model is coupled with the geochemical code PHREEQC, thus providing the flexibility of simulating a wide variety geochemical reactions included in the PHREEQC package. Two-dimensional conservative and reactive (ion-exchange) transport scenarios were presented to demonstrate the capability of the developed model to simulate multicomponent ionic transport in physically and chemically heterogeneous formations. The simulations were performed in a homogeneous porous medium at laboratory scale, as well as in heterogeneous porous media at the field scale. The simulation outcomes show that the micro-scale physical (diffusion/dispersion) and/or electrochemical processes (Coulombic interactions) significantly affect the macro-scale transport and dilution both in the homogeneous and in the heterogeneous domains. For conservative transport, the results of this study show that the coupling effects of charge interactions can be appreciated from the 2-D distribution of the different ions and quantified using metrics of mixing such as the flux-related dilution index. However, such effects might be overlooked by only analyzing flux-averaged concentration breakthrough curves. Furthermore, mapping the different components of the dispersive fluxes is also very useful to understand and visualize the Coulombic coupling between the different ions and the effects of electrochemical migration. The impact of electrostatic interactions is also shown to be significant for the evolution of reactive plumes undergoing cation exchange in physically and geochemically heterogeneous domains. For these scenarios we found

that the two-dimensional concentration distributions of the transported ions, as well as their integrated breakthrough curves at the outlet, are affected by the electrochemical migration terms coupling the transport of the charged species. Such effects influence the displacement of the dissolved ions in the pore water as well as their interaction with the solid matrix, since a different displacement compared to the “liberated state” causes the ions to interact with different reactive zones of the porous medium.

Besides the specific scenarios investigated in this study, the proposed multicomponent ionic transport code can be used to explore the effects of Coulombic interactions in porous media in a wide variety of reactive transport problems. This can include mineral precipitation and dissolution, sorption and surface complexation reactions, propagation of pH fronts, mobilization of heavy metals and metalloids and biodegradation reactions (e.g., [84-90]). We think that the code offers particular advantages for the study of transport and Coulombic interactions in flow-through systems when the aim is to provide a detailed description of the effects of physical and chemical heterogeneity. The current model formulation is limited to multicomponent ionic transport of dilute solutions in two-dimensional formations. Further work is required to extend the framework to systems with strong gradients of ionic strength and to three-dimensional transport problems. For fully 3-D transport, recent experimental studies have shown a more pronounced effect of diffusion and compound-specific dispersion on solute displacement and plume dilution [45]. Therefore, under these conditions, the effects of Coulombic interactions on the displacement of charged species are expected to be more pronounced compared to two-dimensional systems. Furthermore, in fully three-dimensional anisotropic heterogeneous porous media, the topology of the flow field and the possible development of twisting

streamlines may play a major role on solute transport [91-93] and, thus, will also be of interest for multicomponent ionic transport problems.

Acknowledgments

This work was supported by the Baden-Württemberg Stiftung under the Eliteprogram for Postdocs. We would like to thank Prof. O. A. Cirpka (University of Tübingen) for discussion and for providing an early version of the streamline oriented code.

References

- [1] Steefel CI, Appelo CAJ, Arora B, Jacques D, Kalbacher T, Kolditz O, Yeh GT. Reactive transport codes for subsurface environmental simulation. *Computat Geosci* 2015; 19:445-78. doi: 10.1007/s10596-014-9443-x.
- [2] Barry DA, Prommer H, Miller CT, Engesgaard P, Brun A, Zheng C. Modelling the fate of oxidisable organic contaminants in groundwater. *Adv Water Resour* 2002;25: 945-83. doi: [http://dx.doi.org/10.1016/S0309-1708\(02\)00044-1](http://dx.doi.org/10.1016/S0309-1708(02)00044-1).
- [3] Steefel CI, Lasaga AC. A coupled model for transport of multiple chemical-species and kinetic precipitation dissolution reactions with application to reactive flow in single-phase hydrothermal systems. *Am Journal Sci* 1994;294:529-92.
- [4] Bethke C. Modelling transport in reacting geochemical systems. *CR Acad Sci Li A* 1997;324:513-28.
- [5] Prommer H, Barry DA, Zheng C. MODFLOW/MT3DMS-based reactive multicomponent transport modeling. *Ground Water* 2003, 41, 247–257.
- [6] Parkhurst DL, Kipp KL, Engesgaard P, Charlton SR. PHAST - A program for simulating ground-water flow, solute transport, and multicomponent geochemical reactions. *Geochim Cosmochim Acta* 2005; 69.
- [7] Yeh GT, VS Tripathi. HYDROGEOCHEM: A coupled model HYDROlogical transport and GEOCHEMical equilibrium of multi component systems. ORNL 6371, Oak Ridge National Laboratory 1990.
- [8] Xu T, Pruess K. Modeling multiphase non-isothermal fluid flow and reactive geochemical transport in variably saturated fractured rocks 1: Methodology. *Am J Sci* 2001;301:16-33, doi: 10.2475/ajs.301.1.16.
- [9] Xu T, Sonnenthal E, Spycher N, Pruess K. TOUGHREACT—A simulation program for non-isothermal multiphase reactive geochemical transport in variably saturated geologic media: Applications to geothermal injectivity and CO₂ geological sequestration. *Comput Geosci* 2006;32:145-65. doi: <http://dx.doi.org/10.1016/j.cageo.2005.06.014>.
- [10] Xu T, Spycher N, Sonnenthal E, Zhang G, Zheng L, Pruess K. TOUGHREACT Version 2.0: A simulator for subsurface reactive transport under non-isothermal multiphase flow conditions. *Comput Geosci* 2011;37:763-74. doi: <http://dx.doi.org/10.1016/j.cageo.2010.10.007>.

745 [11] Mayer KU, Frind EO, Blowes DW. Multicomponent reactive transport modeling in
 746 variably saturated porous media using a generalized formulation for kinetically controlled
 747 reactions. *Water Resour Res* 2002;38:1301-21. doi: 10.1029/2001WR000862.

748 [12] Šimunek J, Jacques D, Šejna M, Van Genuchten MT. The HP2 program for
 749 HYDRUS (2D/3D): A coupled code for simulating two-dimensional variably-saturated
 750 water flow, heat transport, and biogeochemistry in porous media, Version 1.0. PC
 751 Progress, Prague, Czech Republic 2012:76.

752 [13] Mao X, Prommer H, Barry DA, Langevin CD, Panteleit B, Li L. Three-dimensional
 753 model for multi-component reactive transport with variable density groundwater flow.
 754 *Environ Model Softw* 2006;21:615-28. doi:
 755 <http://dx.doi.org/10.1016/j.envsoft.2004.11.008>.

756 [14] Wissmeier L, Barry DA. Implementation of variably saturated flow into PHREEQC
 757 for the simulation of biogeochemical reactions in the vadose zone. *Environ Model Softw*
 758 2010;25:526-38. doi: <http://dx.doi.org/10.1016/j.envsoft.2009.10.001>.

759 [15] Charlton SR, Parkhurst DL. Modules based on the geochemical model PHREEQC
 760 for use in scripting and programming languages. *Comput Geosci* 2011;37:1653-63. doi:
 761 <http://dx.doi.org/10.1016/j.cageo.2011.02.005>.

762 [16] Parkhurst DL, Wissmeier L. PhreeqcRM: A reaction module for transport simulators
 763 based on the geochemical model PHREEQC. *Adv Water Resour* 2015;83:176-89. doi:
 764 <http://dx.doi.org/10.1016/j.advwatres.2015.06.001>.

765 [17] Parkhurst DL, Appelo CAJ. User's guide to PHREEQC (Version 2) - A computer
 766 program for speciation, batch-reaction, one-dimensional transport, and inverse
 767 geochemical calculations. U.S. Geological Survey Water Resources Investigations Report
 768 1999; 99-4259.

769 [18] Parkhurst DL, Appelo CAJ. Description of input and examples for PHREEQC
 770 version 3- A computer program for speciation, batch-reaction, one dimensional transport,
 771 and inverse geochemical calculations. U.S. Geological Survey Techniques and Methods
 772 2013;6-A43:497. available only at <http://pubs.usgs.gov/tm/06/a43/>.

773 [19] Wissmeier L, Barry DA. Simulation tool for variably saturated flow with
 774 comprehensive geochemical reactions in two- and three-dimensional domains. *Environ*
 775 *Model Softw* 2011;26:210-8. doi: <http://dx.doi.org/10.1016/j.envsoft.2010.07.005>.

776 [20] Müller M, Parkhurst DL, Charlton SR. Programming PHREEQC calculations with
 777 C++ and Python - A comparative study. In: Maxwell R, Poeter E, Hill M, Zheng C,
 778 MODFLOW and More 2011 - Integrated Hydrological Modeling Proceedings 2011:632-
 779 636.

780 [21] Nardi A, Idiart A, Trinchero P, de Vries LM, Molinero J. Interface COMSOL-
 781 PHREEQC (iCP), an efficient numerical framework for the solution of coupled
 782 multiphysics and geochemistry. *Comput Geosci* 2014;69:10-21. doi:
 783 <http://dx.doi.org/10.1016/j.cageo.2014.04.011>.

784 [22] Nasir O, Fall M, Evgin E. A simulator for modeling of porosity and permeability
 785 changes in near field sedimentary host rocks for nuclear waste under climate change
 786 influences. *Tunn Undergr Sp Tech* 2014;42:122-35. doi:
 787 <http://dx.doi.org/10.1016/j.tust.2014.02.010>.

788 [23] Kolditz O, Bauer S, Bilke L, Böttcher N, Delfs JO, Fischer T, Zehner B.
 789 OpenGeoSys: An open-source initiative for numerical simulation of thermo-hydro-

mechanical/chemical (THM/C) processes in porous media. *Environ Earth Sci* 2012;67:589-99. doi: 10.1007/s12665-012-1546-x.

[24] He W, Beyer C, Fleckenstein JH, Jang E, Kolditz O, Naumov D, Kalbacher T. A parallelization scheme to simulate reactive transport in the subsurface environment with OGS#IPhreeqc 5.5.7-3.1.2. *Geosci Model Dev* 2015;8:3333-48. doi: 10.5194/gmd-8-3333-2015.

[25] Korrani AKN, Sepehrnoori K, Delshad M. Coupling IPhreeqc with UTCHEM to model reactive flow and transport. *Comput Geosci* 2015;82:152-69, doi: <http://dx.doi.org/10.1016/j.cageo.2015.06.004>.

[26] Vinograd JR, McBain JW. Diffusion of electrolytes and of the ions in their mixtures. *J Am Chem Soc* 1941;63:2008-15. doi: 10.1021/ja01852a063.

[27] Liu CX, Shang JY, Zachara JM. Multispecies diffusion models: A study of uranyl species diffusion. *Water Resour Res* 2011; 47: W12514. <http://dx.doi.org/10.1029/2011WR010575>.

[28] Giambalvo ER, Steefel CI, Fisher AT, Rosenberg ND, Wheat CG. Effect of fluid-sediment reaction on hydrothermal fluxes of major elements, eastern flank of the Juan de Fuca Ridge. *Geochim Cosmochim Acta* 2002;66:1739-57. doi: [10.1016/S0016-7037\(01\)00878-X](https://doi.org/10.1016/S0016-7037(01)00878-X).

[29] Appelo CAJ, Wersin P. Multicomponent diffusion modeling in clay systems with application to the diffusion of tritium, iodide, and sodium in opalinus clay. *Environ Sci Tech* 2007;41:5002-7. doi: Doi 10.1021/Es0629256.

[30] Appelo CAJ, Vinsot A, Mettler S, Wechner S. Obtaining the porewater composition of a clay rock by modeling the in- and out-diffusion of anions and cations from an in-situ experiment. *J Contam Hydrol* 2008;101:67-76. doi: DOI 10.1016/j.jconhyd.2008.07.009.

[31] Appelo CAJ, Van Loon LR, Wersin P. Multicomponent diffusion of a suite of tracers (HTO, Cl, Br, I, Na, Sr, Cs) in a single sample of Opalinus Clay. *Geochim Cosmochim Acta* 2010;74:1201-19. doi: 10.1016/j.gca.2009.11.013.

[32] Ben-Yaakov S. Diffusion of sea water ions—I. Diffusion of sea water into a dilute solution. *Geochim Cosmochim Acta* 1972;36:1395-406. doi: 10.1016/0016-7037(72)90069-5.

[33] Lasaga AC. The treatment of multi-component diffusion and ion pairs in diagenetic fluxes. *Am J Sci* 1979;279:324-46. doi: 10.2475/ajs.279.3.324.

[34] Felmy AR, Weare JH. Calculation of multicomponent ionic-diffusion from zero to high-concentration 1. The System Na-K-Ca-Mg-Cl-SO₄-H₂O at 25-degrees-C. *Geochim Cosmochim Acta* 1991;55:113-31. doi: Doi 10.1016/0016-7037(91)90405-T.

[35] Boudreau BP, Meysman FJR, Middelburg JJ. Multicomponent ionic diffusion in porewaters: Coulombic effects revisited. *Earth Planet Sci Lett* 2004;222:653-66. doi: 10.1016/j.epsl.2004.02.034.

[36] Cussler EL. *Diffusion : Mass transfer in fluid systems*. 3rd ed. Cambridge University Press, Cambridge, New York 2009.

[37] Rolle M, Muniruzzaman M, Haberer CM, Grathwohl P. Coulombic effects in advection-dominated transport of electrolytes in porous media: Multicomponent ionic dispersion. *Geochim Cosmochim Acta* 2013;120:195-205. doi: <http://dx.doi.org/10.1016/j.gca.2013.06.031>.

[38] Muniruzzaman M, Haberer CM, Grathwohl P, Rolle M. Multicomponent ionic dispersion during transport of electrolytes in heterogeneous porous media: Experiments

and model-based interpretation. *Geochim Cosmochim Acta* 2014;141:656-69. doi: <http://dx.doi.org/10.1016/j.gca.2014.06.020>.

[39] Muniruzzaman M, Rolle M. Impact of multicomponent ionic transport on pH fronts propagation in saturated porous media. *Water Resour Res* 2015;51:6739-55. doi: 10.1002/2015WR017134.

[40] Rasouli P, Steefel CI, Mayer KU, Rolle M. Benchmarks for multicomponent diffusion and electrochemical migration. *Computat Geosci* 2015;19:523-33. doi: 10.1007/s10596-015-9481-z.

[41] Bauer RD, Rolle M, Bauer S, Eberhardt C, Grathwohl P, Kolditz O, Griebler C. Enhanced biodegradation by hydraulic heterogeneities in petroleum hydrocarbon plumes. *J Contam Hydrol* 2009;105:56-68. doi: 10.1016/j.jconhyd.2008.11.004.

[42] Rolle M, Chiogna G, Bauer R, Griebler C, Grathwohl P. Isotopic fractionation by transverse dispersion: Flow-through microcosms and reactive transport modeling study. *Environ Sci Tech* 2010;44:6167-73. doi: 10.1021/es101179f.

[43] Haberer CM, Rolle M, Cirpka OA, Grathwohl P. Oxygen transfer in a fluctuating capillary fringe. *Vadose Zone J* 2012;11. doi: 10.2136/Vzj2011.0056.

[44] Hochstetler DL, Rolle M, Chiogna G, Haberer CM, Grathwohl P, Kitanidis PK. Effects of compound-specific transverse mixing on steady-state reactive plumes: Insights from pore-scale simulations and Darcy-scale experiments. *Adv Water Resour* 2013;54:1-10. doi: 10.1016/j.advwatres.2012.12.007.

[45] Ye Y, Chiogna G, Cirpka OA, Grathwohl P, Rolle M. Enhancement of plume dilution in two-dimensional and three-dimensional porous media by flow focusing in high-permeability inclusions. *Water Resour Res* 2015;51:5582-602. doi: 10.1002/2015WR016962.

[46] Fiori A, Jankovic I, Dagan G. The impact of local diffusion upon mass arrival of a passive solute in transport through three-dimensional highly heterogeneous aquifers. *Adv Water Resour* 2011;34:1563-73. doi: 10.1016/j.advwatres.2011.08.010.

[47] Hadley PW, Newell C. The new potential for understanding groundwater contaminant transport. *Groundwater* 2014;52:174-86. doi: 10.1111/gwat.12135.

[48] LaBolle EM, Fogg GE. Role of molecular diffusion in contaminant migration and recovery in an alluvial aquifer system. *Trans Porous Med* 2001;42:155-79. doi: 10.1023/A:1006772716244.

[49] Liu CX, Ball WP. Back diffusion of chlorinated solvent contaminants from a natural aquitard to a remediated aquifer under well-controlled field conditions: Predictions and measurements. *Ground Water* 2002;40:175-84. doi: 10.1111/j.1745-6584.2002.tb02502.x.

[50] Chiogna G, Eberhardt C, Grathwohl P, Cirpka OA, Rolle M. Evidence of compound-dependent hydrodynamic and mechanical transverse dispersion by multitracer laboratory experiments. *Environ Sci Tech* 2010;44:688-93. doi: 10.1021/Es9023964.

[51] Chiogna G, Cirpka OA, Grathwohl P, Rolle M. Relevance of local compound-specific transverse dispersion for conservative and reactive mixing in heterogeneous porous media. *Water Resour Res* 2011;47:W07540. doi: 10.1029/2010wr010270.

[52] Rasa E, Chapman SW, Bekins BA, Fogg GE, Scow KM, Mackay DM. Role of back diffusion and biodegradation reactions in sustaining an MTBE/TBA plume in alluvial media. *J Contam Hydrol* 2011;126:235-47. doi: <http://dx.doi.org/10.1016/j.jconhyd.2011.08.006>.

- [53] Rolle M, Chiogna G, Hochstetler DL, Kitanidis PK. On the importance of diffusion and compound-specific mixing for groundwater transport: An investigation from pore to field scale. *J Contam Hydrol* 2013;153:51-68. <http://dx.doi.org/10.1016/j.jconhyd.2013.07.006>.
- [54] Van Breukelen BM, Rolle M. Transverse hydrodynamic dispersion effects on isotope signals in groundwater chlorinated solvents' plumes. *Environ Sci Tech* 2012;46:7700-8. doi: 10.1021/es301058z.
- [55] Kitanidis PK. The concept of the Dilution Index. *Water Resour Res* 1994;30:2011-26. doi: 10.1029/94WR00762.
- [56] Van Cappellen P, J-F Gaillard. Biogeochemical dynamics in aquatic sediments. *Reviews in Mineralogy and Geochemistry*. 34 (1996) 335-76.
- [57] Liu CX, Zachara JM, Felmy AR, Gorby Y. An electrostatics-based model for ion diffusion in microbial polysaccharides. *Colloids Surf A and B* 2004;38:55-65. doi: 10.1016/j.colsurfb.2004.08.003.
- [58] Alizadeh A, Zhang L, Wang MR. Mixing enhancement of low-Reynolds electro-osmotic flows in microchannels with temperature-patterned walls. *J Colloid Interface Sci* 2014;431:50-63. doi: 10.1016/j.jcis.2014.05.070.
- [59] Zhang L, Wang MR. Modeling of electrokinetic reactive transport in micropore using a coupled lattice Boltzmann method. *J Geophys Res-Sol Ea* 2015;120:2877-90. doi: 10.1002/2014JB011812.
- [60] Bard AJ, Faulkner LR. *Electrochemical methods fundamentals and applications*. (2nd ed.). John Wiley, New York 2001:718.
- [61] Cirpka OA, Frind EO, Helmig R. Streamline-oriented grid generation for transport modelling in two-dimensional domains including wells. *Adv Water Resour* 1999;22:697-710. doi: 10.1016/S0309-1708(98)00050-5.
- [62] Guedes de Carvalho JRF, Delgado JMPQ. Overall map and correlation of dispersion data for flow through granular packed beds. *Chem Eng Sci* 2005;60:365-75. doi: <http://dx.doi.org/10.1016/j.ces.2004.07.121>.
- [63] Rolle M, Hochstetler DL, Chiogna G, Kitanidis PK, Grathwohl P. Experimental investigation and pore-scale modeling interpretation of compound-specific transverse dispersion in porous media. *Trans Porous Med* 2012;93:347-62. doi: 10.1007/s11242-012-9953-8.
- [64] Archie GE. The electrical resistivity log as an aid in determining some reservoir characteristics. *Trans AIME*; 146.
- [65] Boving TB, P Grathwohl. Tracer diffusion coefficients in sedimentary rocks: correlation to porosity and hydraulic conductivity. *J Contam Hydrol* 2001; 53:85-100. doi: Doi 10.1016/S0169-7722(01)00138-3.
- [66] Scheidegger AE. General theory of dispersion in porous media. *Journal of Geophys Res* 1961;66:3273-8. doi: 10.1029/JZ066i010p03273.
- [67] Bijeljic B, Muggeridge AH, Blunt MJ. Pore-scale modeling of longitudinal dispersion. *Water Resour Res* 2004;40:W11501. doi: 10.1029/2004wr003567.
- [68] Hazen A. Some physical properties of sands and gravels: with special reference to their use in filtration. *Ann Rep State Board of Health Mass* 1892;24:541-556.
- [69] Eckert D, Rolle M, Cirpka OA. Numerical simulation of isotope fractionation in steady-state bioreactive transport controlled by transverse mixing. *J Contam Hydrol* 2012;140-141:95-106. doi: <http://dx.doi.org/10.1016/j.jconhyd.2012.08.010>.

928 [70] Cirpka OA, Frind EO, Helmig R. Numerical methods for reactive transport on
929 rectangular and streamline-oriented grids. *Adv Water Resour* 199;22:711-28.
930 [http://dx.doi.org/10.1016/S0309-1708\(98\)00051-7](http://dx.doi.org/10.1016/S0309-1708(98)00051-7).

931 [71] Davis T, Duff I. An unsymmetric-pattern multifrontal method for sparse LU
932 factorization. *SIAM J Matrix Anal* 1997;18:140-58. doi: 10.1137/S0895479894246905.

933 [72] Leij FJ, Skaggs TH, van Genuchten MT. Analytical solutions for solute transport in
934 three-dimensional semi-infinite porous media. *Water Resour Res* 1991;27:2719-33. doi:
935 10.1029/91WR01912.

936 [73] van Genuchten MT, Leij FJ, Skaggs TH, Toride N, Bradford SA, Pontedeiro EM.
937 Exact analytical solutions for contaminant transport in rivers 1. The equilibrium
938 advection-dispersion equation. *J Hydrol Hydromech* 2013;61:146-60. doi: 10.2478/johh-
939 2013-0020.

940 [74] Lasaga AC. *Kinetic theory in the earth sciences*. Princeton University Press,
941 Princeton, N.J 1998.

942 [75] Tartakovsky AM, Redden G, Lichtner PC, Scheibe TD, Meakin P. Mixing-induced
943 precipitation: Experimental study and multiscale numerical analysis. *Water Resour Res*
944 2008;44:W06s04. doi: 10.1029/2006wr005725.

945 [76] Rolle M, Eberhardt C, Chiogna G, Cirpka OA, Grathwohl P. Enhancement of
946 dilution and transverse reactive mixing in porous media: Experiments and model-based
947 interpretation. *J Contam Hydrol* 2009;110:130-42. doi: 10.1016/j.jconhyd.2009.10.003.

948 [77] Rolle M, Kitanidis PK. Effects of compound-specific dilution on transient transport
949 and solute breakthrough: A pore-scale analysis. *Adv Water Resour* 2014;71:186-99.
950 <http://dx.doi.org/10.1016/j.advwatres.2014.06.012>.

951 [78] Sudicky EA. A natural gradient experiment on solute transport in a sand aquifer:
952 Spatial variability of hydraulic conductivity and its role in the dispersion process. *Water*
953 *Resour Res* 1986;22:2069-82. doi: 10.1029/WR022i013p02069.

954 [79] Dykaar BB, Kitanidis PK. Determination of the effective hydraulic conductivity for
955 heterogeneous porous media using a numerical spectral approach: 1. Method. *Water*
956 *Resour Res*. 1992;28:1155-66. doi: 10.1029/91WR03084.

957 [80] Yang C, J Samper. Numerical evaluation of multicomponent cation exchange
958 reactive transport in physically and geochemically heterogeneous porous media.
959 *Computat Geosci* 2009;13:391-404. doi: 10.1007/s10596-009-9127-0.

960 [81] Christiansen JS, Engesgaard PK, Bjerg PL. A physically and chemically
961 heterogeneous aquifer: field study and reactive transport modelling. In: *Groundwater*
962 *Quality: Remediation and Protection, Proceedings of the GQ'98 Conference*, IAHS Press,
963 Wallingford 1998:329-36.

964 [82] Jacques D, Mouvet C, Mohanty B, Vereecken H, Feyen J. Spatial variability of
965 atrazine sorption parameters and other soil properties in a podzoluvisol. *J Contam Hydrol*
966 1999;36:31-52. [http://dx.doi.org/10.1016/S0169-7722\(98\)00141-7](http://dx.doi.org/10.1016/S0169-7722(98)00141-7).

967 [83] Samper J, Yang C. Stochastic analysis of transport and multicomponent competitive
968 monovalent cation exchange in aquifers. *Geosphere* 2006;2:102-12. doi:
969 10.1130/ges00030.1.

970 [84] Kjølner C, Postma D, Larsen F. Groundwater acidification and the mobilization of
971 trace metals in a sandy aquifer. *Environ Sci Tech* 2004;38:2829-35. doi:
972 10.1021/es030133v.

- [85] Prigiobbe V, Bryant SL. pH-dependent transport of metal cations in porous media. *Environ Sci Tech* 2014;48:3752-9. doi: 10.1021/es403695r.
- [86] Li L, Salehikhoo F, Brantley SL, Heidari P. Spatial zonation limits magnesite dissolution in porous media. *Geochim Cosmochim Acta* 2014;126:555-73. <http://dx.doi.org/10.1016/j.gca.2013.10.051>.
- [87] Molins S, Trebotich D, Steefel CI, Shen CP. An investigation of the effect of pore scale flow on average geochemical reaction rates using direct numerical simulation. *Water Resour Res* 2012;48:W03527. doi: 10.1029/2011wr011404.
- [88] Haberer CM, Muniruzzaman M, Grathwohl P, Rolle M. Diffusive/Dispersive and reactive fronts in porous media: Fe (II)-Oxidation at the unsaturated/saturated interface. *Vadose Zone J* 2015;14(5). doi: <http://dx.doi.org/10.2136/vzj2014.07.0091>.
- [89] Fakhreddine S, Lee J, Kitanidis PK, Fendorf S, Rolle M. Imaging geochemical heterogeneities using inverse reactive transport modeling: An example relevant for characterizing arsenic mobilization and distribution. *Adv Water Resour* 2016;88: 186-97. <http://dx.doi.org/10.1016/j.advwatres.2015.12.005>.
- [90] Redden G, Fox D, Zhang C, Fujita Y, Guo L, Huang H. CaCO₃ precipitation, transport and sensing in porous media with in situ generation of reactants. *Environ Sci Tech* 2014;48:542-9. doi: 10.1021/es4029777.
- [91] Chiogna G, Rolle M, Bellin A, Cirpka OA. Helicity and flow topology in three-dimensional anisotropic porous media. *Adv Water Resour* 2014;73:134-43. <http://dx.doi.org/10.1016/j.advwatres.2014.06.017>.
- [92] Ye Y, G Chiogna, OA Cirpka, P Grathwohl, M Rolle. experimental evidence of helical flow in porous media. *Phys Rev Lett* 2015;115:194502. doi: 10.1103/Physrevlett.115.194502.
- [93] Cirpka OA, Chiogna G, Rolle M, Bellin A. Transverse mixing in three-dimensional nonstationary anisotropic heterogeneous porous media. *Water Resour Res* 2015;51:241-60. doi: 10.1002/2014WR015331.

1000